Assessing ocean buoy shortwave observations using clear-sky model calculations

M. Medovaya and D. E. Waliser
Marine Sciences Research Center, State University of New York at Stony Brook, Stony Brook, New York, USA

R. A. Weller
Woods Hole Oceanographic Institution, Woods Hole, Massachusetts, USA

M. J. McPhaden
Pacific Marine Environmental Laboratory, Seattle, Washington, USA

Received 19 July 2000; revised 29 June 2001; accepted 25 July 2001; published 28 February 2002.

[1] Comparison of ocean buoy observations and model calculations of incoming clear-sky surface shortwave radiation is performed in order to assess the buoys' general reliability under operating conditions. The buoy data employed for this study come from several experimental and operational deployments conducted by Woods Hole Oceanographic Institution (WHOI) and Pacific Marine Environmental Laboratory (PMEL). WHOI deployments include the Frontal Air-Sea Interaction Experiment, Marine Light Mixed Layer Experiment, Coupled Ocean-Atmosphere Response, Subduction Experiment, Arabian Sea Experiment, Pan-American Climate Study, and Biowatt. PMEL deployments include the Tropical Atmosphere Ocean moored buoy array in the tropical Pacific Ocean. These moorings and their associated shortwave measurements represent the vast majority of open-ocean in situ shortwave observations available to date. Two separate schemes were used to filter the cloudy samples from the buoy shortwave time series, one based on satellite values of cloudiness and a second scheme based on the buoy observations themselves and on a number of additional constraints. The clear-sky model calculations of surface shortwave were computed using the single-column radiation code from the National Center for Atmospheric Research Community Climate Model, version 3. The primary uncertainty associated with the model calculations is the specification of the aerosol amount. In general, there was a fairly high level of agreement between the buoy and modeled values of clear-sky surface shortwave. However, there were a few buoys that exhibited significant model-data discrepancies (e.g., model-data biases exceeding 10%, or $\sim$40 W m^{-2}). The possible reasons for these discrepancies were investigated. In some cases, unaccounted for aerosol variability in the model was found to be the most probable cause, indicating that observations were likely to be reliable. In other cases, the discrepancies appeared to result from sensor tilt associated with wind, currents, or deployment/mounting problems and/or were possibly due to aerosol buildup on the sensor. *INDEX TERMS:* 3359 Meteorology and Atmospheric Dynamics: Radiative processes; 4294 Oceanography: General: Instruments and techniques; 4504 Oceanography: Physical: Air/sea interactions (0312); *KEYWORDS:* clear-sky model, ocean, ocean buoy, shortwave radiation

1. Introduction

[2] Solar energy accounts for most, if not all, of the positive heat flux transferred into the ocean across the air-sea interface. In this regard, the significance of solar energy in the climate system is undeniable, and it is therefore imperative that general circulation models (GCMs), especially those with interactive oceans and sea ice, properly model solar radiative transfer. A large amount of effort has been undertaken to correctly account for the incoming solar fluxes in numerical weather forecasting and climate simulations/predictions. This is an especially difficult endeavor because of the complex nature of clouds that, aside from the diurnal and annual cycle, provide the largest spatial and temporal modulation to shortwave (SW) radiation in the climate system [e.g., *Cess et al.*, 1989; *Harrison et al.*, 1990; *Arking*, 1991]. Difficulty also arises because of shortcomings in portraying spatial and temporal distributions of aerosols and gases and parameterizing their radiative properties accurately [e.g., *Slingo and Slingo*, 1991; *Ramaswamy and Freidenreich*, 1992; *Kiehl and Briegleb*, 1993].

[3] One significant limitation on pursuing the above line of research and development is the lack of SW validation data readily available over the ocean. Having such validation data is critical because of the large area of the planet's surface covered by ocean and because ocean regions often exhibit atmospheric conditions (e.g., cloud types or aerosol characteristics) different from their continental counterpart. Validation to date has largely consisted of the ship-derived values using qualitative cloud report data [e.g., *Weare et al.*, 1980; *Esbensen and Kushnir*, 1981; *Oberhuber*, 1988] or land-based data, such as the Global Energy Balance Archive [*Ohmura and Gilgen*, 1991], the Baseline Surface Radiation Network [*Ohmura et al.*, 1998], or data from field experiments such as the First International Satellite Cloud Climatology Project Regional Experiment or the Atmospheric Radiation Measurement (ARM) program. It is important to note that few, if any, of the above represent true open-ocean conditions monitored with well-calibrated radiometers.

0148-0227/02/2000JC000558$09.00

[4] To help address this lack of open-ocean validation data for surface SW, a number of buoy deployments have been carried out over the last decade that included SW observations. For the most part, these observations were part of the experiments and monitoring projects conducted by the National Oceanic and Atmospheric Administration Pacific Marine Environmental Laboratory (PMEL) and the Woods Hole Oceanographic Institution (WHOI). While our capabilities in the area of buoy-measured radiation are growing, uncertainties still exist regarding the accuracy of these measurements because of the stressful and remote operational environment of the buoys. Problems are anticipated to arise because of salt and aerosol buildup on the pyranometers, buoy tilting and rocking, calibration drift of the instruments, etc., all of which are potential sources of errors in the SW radiation data measured at the moorings. It is important that these problems, and the associated uncertainties they introduce to the data, are understood and quantified to the extent possible so that these data can be better directed toward their intended applications (e.g., satellite and model validation and heat budget studies). Thus the intent of this study is to try and examine the quality and reliability of the available ocean buoy SW observations under operating conditions, i.e., throughout the length of deployment. Such an analysis provides an additional check to the typical calibration procedures performed before and after buoy deployments in more controlled environments.

[5] The assessment of the buoy data is based on comparison of buoy SW data against a benchmark that allows a uniform approach for comparing the disparate set of the observations. In this study, this benchmark is chosen to be the clear-sky surface solar radiation computed from a theoretical radiative transfer algorithm. These computed values of clear-sky radiation can be compared with the actual buoy observations to determine the possible presence and sources of errors in the buoy data. The confidence in the representation of clear-sky SW radiation by the theoretical radiative transfer models is supported by studies such as those performed by *Cess et al.* [1996], *Zender et al.* [1997], and *Jing and Cess* [1998], each of which find good agreement between model-predicted and observed clear-sky SW measured under well maintained and controlled conditions. The nature and results of the comparisons in these studies, as well as a description of the particular model employed for this study, are discussed in section 3.2. As indicated above, the model-data comparisons undertaken in this study are restricted to clear skies because significant uncertainties still exist in the representation of clouds in numerical models and in the theoretical treatment of cloud-radiative interactions [*Slingo and Slingo*, 1991; *Cess et al.*, 1995; *Clough and Brown*, 1995; *Kiehl et al.*, 1995; *Arking*, 1996; *Cess et al.*, 1996; *Fung and Ramaswamy*, 1999]. In addition, in order to assess errors associated with cloudy conditions, it would be necessary to specify cloud observations for the model calculations. However, no robust forms of this type of data are available over the buoy sites. Therefore, by focusing on just clear-sky SW values, vast sources of model uncertainty are eliminated, and the main objective of the study can still be carried out.

[6] In section 2 the buoy observations are discussed in more detail, and other sources of data used in this study are also discussed briefly. In section 3 the procedures behind the model versus observed clear-sky surface flux comparisons are described. Section 4 presents the results of this comparison. In section 5 the results are summarized and their implications on the utility of the buoy data and future observation efforts are discussed. Additional details associated with this study can be found in the work of *Medovaya* [1999].

2. Data

[7] Figure 1 shows the time periods and the locations of the buoy SW records analyzed in this study. These data come entirely from deployments carried out by WHOI and PMEL, and most of them took place in the 1990s, with the exception of the Frontal Air-Sea Interaction Experiment (FASINEX) and Biowatt. It is important to point out that these deployments and their associated SW measurements represent the vast majority of high-quality open-ocean SW observations to date. Further, several of the deployments consist of exceptionally long time series of SW observations. For example, the Subduction Experiment consists of 2-year time series, and several Tropical Atmosphere-Ocean (TAO) deployments have lasted ~6 years, though there are gaps in the available data due to occasional instrument failures. Such long-running time series of surface SW flux over the open ocean are unprecedented and are extremely valuable for a number of purposes, including validation of satellite and model-derived fluxes, as well as ocean heat budget studies.

2.1. TAO Array

[8] PMEL is in charge of the operation of the TAO moored buoy array in the tropical Pacific Ocean [*McPhaden et al.*, 1998]. SW solar radiation has been measured at several sites within the TAO array [*Mangum et al.*, 1994]. The analysis presented here is focused on the time series from the longest TAO buoy deployments. These include four equatorial buoys located at 110°W, 140°W, 156°E, and 165°E (hereinafter referred to as 0n110w, 0n140w, 0n156e, 0n165e; see Figure 1, solid circles). Each of these provides 4–6 years of data. Figure 1(a) shows that these deployment periods typically lasted from ~1993 to ~1998, although typical time of an individual pyranometer deployment was ~6 months. Note that SW radiation measurements continue to be made at 110°W, 140°W, and 165°E along the equator at the present time.

[9] Each of the TAO buoys was equipped with an Eppley Laboratory precision spectral pyranometer as a SW sensor. The 6-min mean radiation values were recorded at 20-min intervals. These data were internally recorded and were retrieved when the moorings were recovered. Sensors were calibrated by the manufacturer before deployment and, when possible, after recovery. Differences between calibrations averaged 2% over a nominal 6-month deployment. The data were assigned different quality flags by PMEL (see *Freitag et al.* [1994] for more information on data quality), and only the best quality data were used in this study (with flag 2). The data provided for this study have been computed and provided to us using the predeployment calibrations [*Freitag et al.*, 1994]. The use of such predeployment calibrations is another motivation for applying an independent method to assess the quality of the buoy measurements under operating conditions. Other meteorological measurements used from the TAO moorings include air temperature, sea surface temperature, humidity, and wind observations.

2.2. Woods Hole Oceanographic Institution

[10] WHOI has conducted several experiments that included measurements of surface SW radiation. These are (see Figure 1) the FASINEX [*Weller*, 1991], Marine Light Mixed Layer Experiment (MLML) [*Plueddemann et al.*, 1995], Coupled Ocean-Atmosphere Response Experiment (TOGA COARE) [*Weller and Anderson*, 1996], Subduction Experiment [*Brink et al.*, 1995; *Moyer and Weller*, 1997], Arabian Sea Experiment [*Weller et al.*, 1998], Pan American Climate Study (PACS) [*Anderson et al.*, 2000], and Biowatt [*Dickey et al.*, 1993]. The time span of these experiments is over 12 years, starting in 1986 with FASINEX and continuing through 1998 with PACS. Some of these experiments employed a number of buoys. FASINEX consisted of five buoys (FASINEX 845, 846, 847, 848, and 849) located ~20 km apart in the Bermudas at 27°N, 70°W, shown on Figure 1 as an open circle. The Subduction Experiment [*Moyer and Weller*, 1997] consisted as well of five buoys moored northwest of the Sahara desert (Figure 1, five asterisks). The two PACS [*Anderson et al.*, 2000] buoys were located in the eastern tropical Pacific on the same longitude but 13° of latitude apart (Figure 1, squares).

[11] Most of the WHOI buoys carried two complete sets of meteorological sensors, using redundancy to ensure that complete time series of all variables were collected. The two sets used by WHOI researchers are a vector-averaging wind recorder (VAWR)

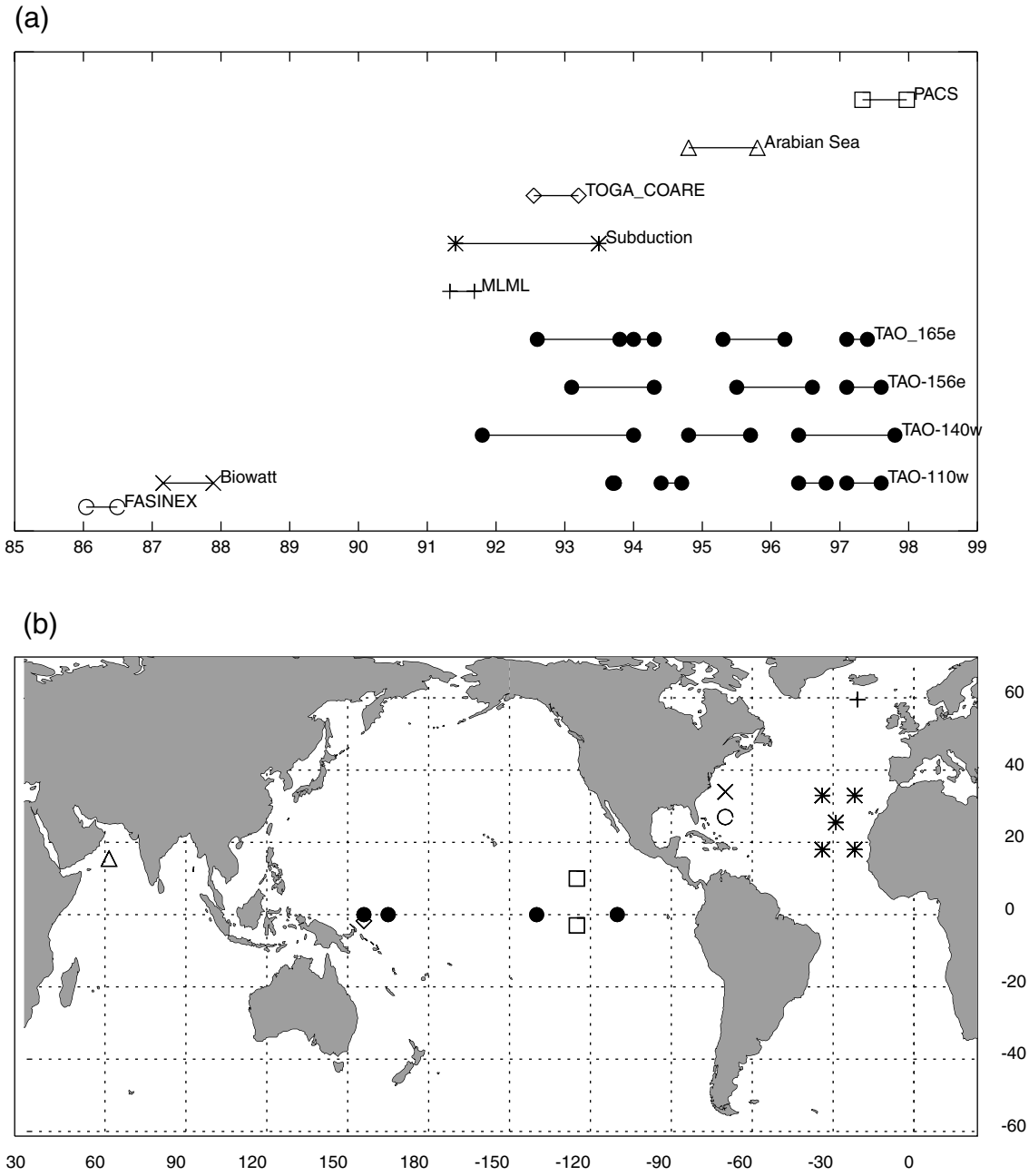

Figure 1. (a) Time periods of Woods Hole Oceanographic Institution (WHOI) and Pacific Marine Environmental Laboratory (PMEL) buoy deployments analyzed in this study. Solid circles indicate PMEL buoys; other symbols indicate WHOI deployments. (b) Map showing the location of the buoy deployments.

and an improved meteorological recorder (IMET). Also, in the case of FASINEX an earlier version of IMET was used: a meteorological recorder (MR). All sets included sensors that also measured barometric pressure, air and sea temperature, relative humidity, and wind speed and direction. Measurements of incoming SW radiation from VAWR and IMET (and MR) systems were made with an Eppley model 8–48 pyranometer and an Eppley precision spectral pyranometer, respectively. The VAWR recorded data once every 7.5 min (FASINEX, Biowatt, TOGA COARE, and Arabian Sea) or 15 min (Subduction, MLML, and PACS), while the IMET recorded data once every 1 min. However, all of the IMET data were subsequently averaged over 7.5- or 15-min intervals to match the recording rate of the VAWR. Sensor performance was evaluated by considering statistics of the differences between like variables observed by the two sets of sensors in comparison to the expected accuracy and precision of the sensors. The best performing sensor for each variable was chosen to form the "final" meteorological data set. In addition, shipboard meteorological observations were made in close proximity to the buoys during deployment/recovery to compare and intercalibrate the ship and buoy measurement systems. The accuracy of the pyranometers employed by the VAWR and IMET systems is within 3% for most of the experiments.

3. Clear-Sky Flux: Observed and Modeled

3.1. Observed Values

[12] Two separate methods are employed to filter cloudy samples from the buoy time series to construct a data set of clear-sky

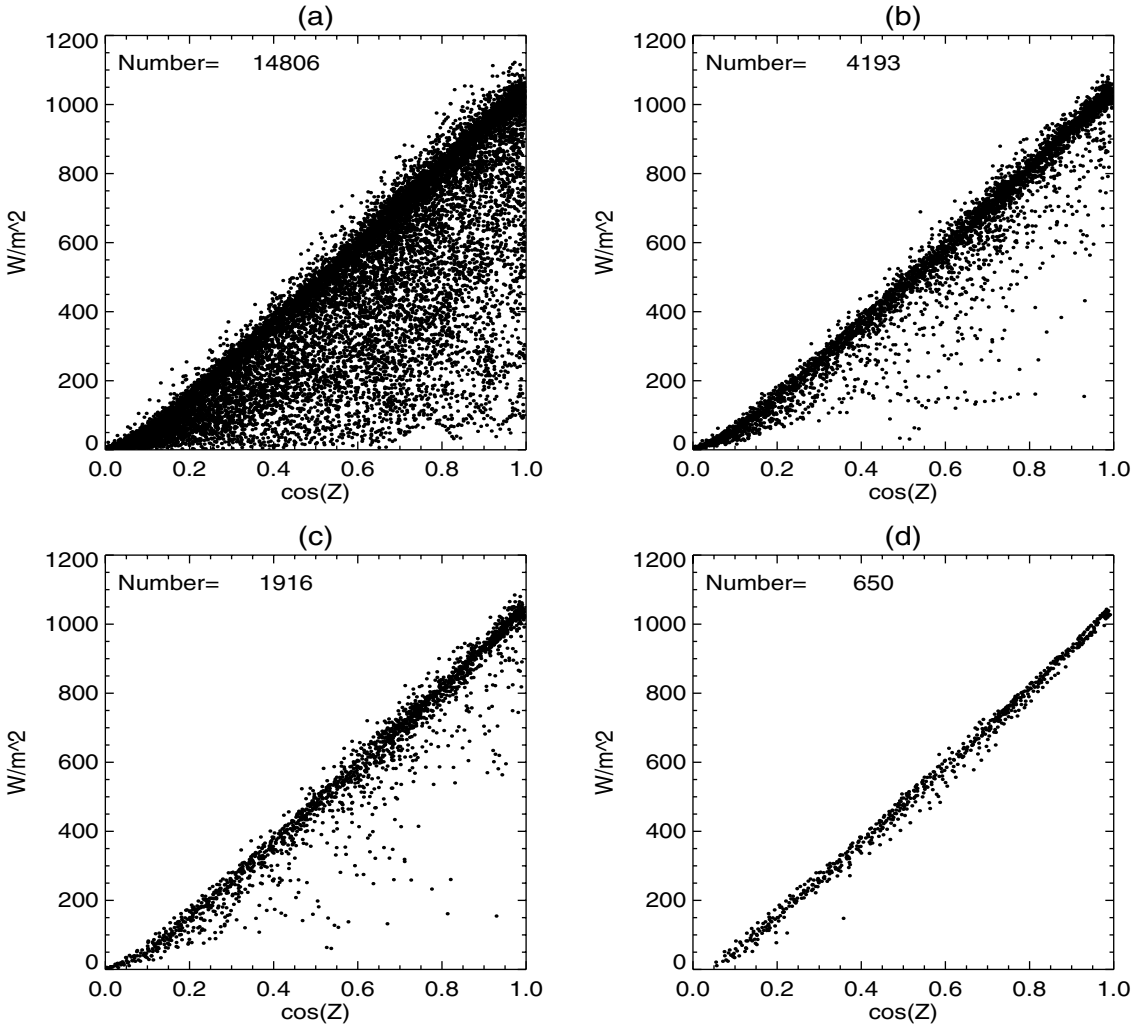

Figure 2. Shortwave (SW) samples from the FASINEX 846 buoy plotted versus the cosine of the solar zenith angle at various stages of the satellite-based cloud-filtering scheme: (a) initial samples available before any filtering, (b) samples remaining after the cloud flag filtering criterion was applied, (c) samples remaining after the reflectance criterion was applied, and (d) samples remaining after the sample-to-sample change criterion was applied. See section 3.1.1.

values. The first uses International Satellite Cloud Climatology Project (ISCCP) DX [*Rossow and Schiffer*, 1991] satellite observations and techniques developed by *Waliser et al.* [1996, 1999], along with additional improvements developed in this study. The second method is necessary for the observations that do not have overlapping satellite retrievals. At the time of this study, ISCCP DX data were only available up to mid-1994, and therefore satellite-based filtering could not be applied to the latter portions of the TAO records or to the PACS and Arabian Sea Experiment since these buoys were deployed after mid-1994 (Figure 1a). Even for the cases where satellite observations were available, the second method was employed to compare the results obtained from each method, since having two separate methods contributes to the confidence in the conclusions from the analysis. The description of these two methods follows in sections 3.1.1 and 3.1.2.

3.1.1. Satellite-based cloud filtering. [13] The satellite-based cloud-filtering method follows, with some modification, the approach developed by *Waliser et al.* [1996, 1999] for deriving the clear-sky flux for the COARE IMET and Subduction buoys. The cloud-filtering scheme utilizes the ISCCP DX data, which have a temporal sampling of 3 hours and a spatial resolution of 30 km, although the data within any one grid cell come from a single (subsampled) satellite pixel with a resolution of ~5 km. The DX quantities used for cloud screening include the cloud detection flag and visible reflectance from the grid cell nearest to the buoy locations. Using these parameters, the cloud screening is performed based on four screening criteria. First, the time of the buoy sample must fall within the 3-hour time span of an ISCCP sample for which the cloud flag for the previous, current, and subsequent ISCCP samples are all equal to zero. This step enforces clear-sky conditions in a large-scale sense over the buoy locations. However, because the satellite footprint is much larger than the buoy radiometer's field of view and because the satellite sample is based on a single instantaneous pixel value representing a 3-hour time period, additional constraints need to be applied in order to filter out small-scale or thin clouds. Figure 2a shows the initial samples in the data set for the FASINEX 846 buoy, and Figure 2b shows the samples remaining after this first criterion is performed. If the filtering step is working correctly, the remaining samples should fall approximately along the "upper envelope" of the initial samples when the data are plotted against the cosine of solar zenith angle (Z), since the clear-sky SW is expected to be the highest possible value at any time of the day (apart from cases of side-lit clouds).

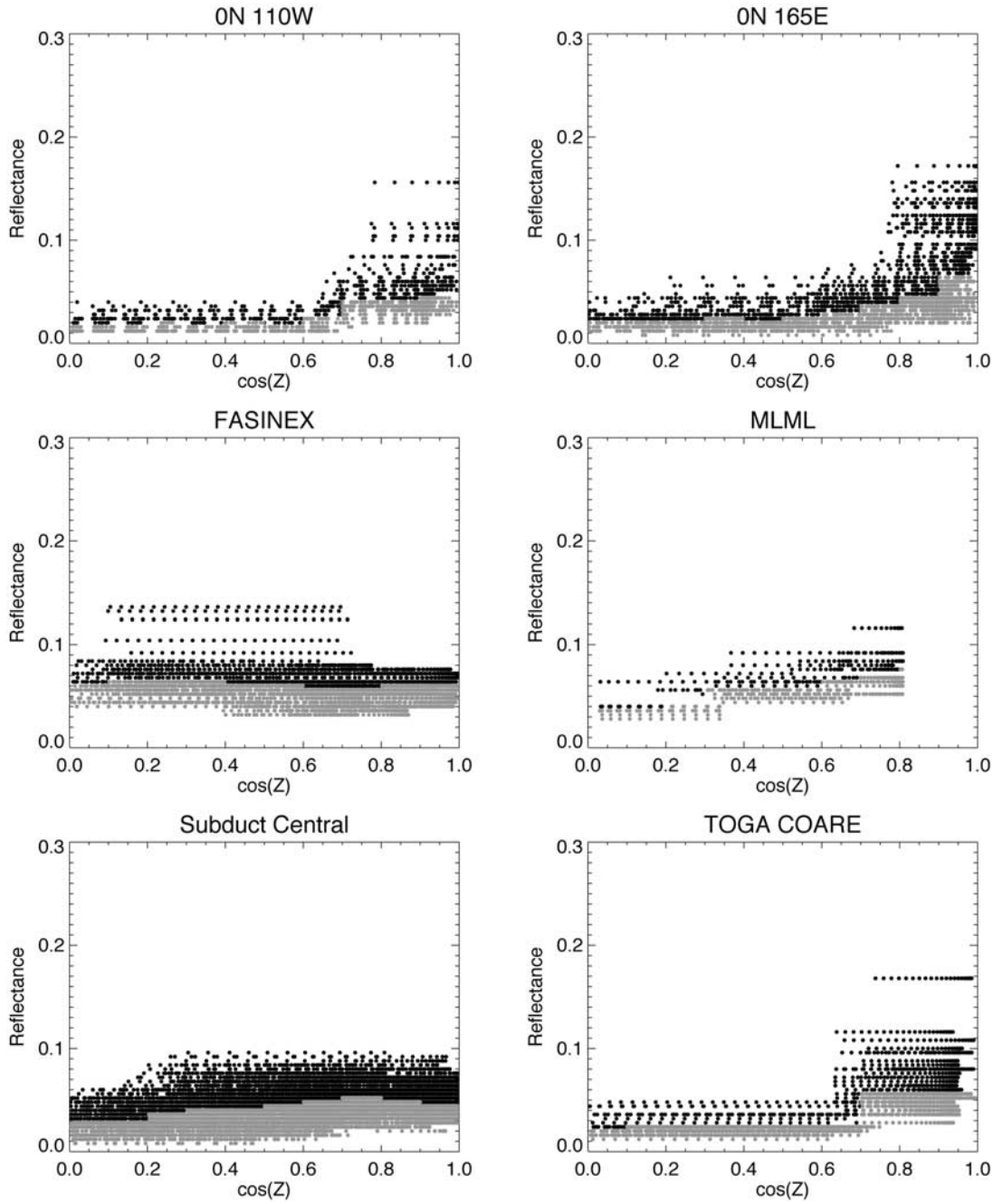

Figure 3. Satellite reflectance values for six different buoys plotted versus the cosine of the solar zenith angle for all the samples remaining (black plus shaded dots) after the satellite-based cloud flag filtering criterion was applied. Black dots are the samples removed by the reflectance criterion. Shaded dots are the samples retained after application of the reflectance criterion.

[14] The second screening criterion is based on lowering the allowed values of the satellite-retrieved visible reflectance values. Reflectance is a function of the surface, solar zenith, and satellite zenith angles. Since the ocean is generally much less reflective than clouds, the lower the reflectance values, the larger the probability that the underlying surface is the ocean rather than a cloud. This criterion simply decreases the likelihood of contamination by isolated or thin clouds, which were not identified by satellite cloud detection. Thus SW radiation samples that have relatively high reflectance values are assumed to be the most likely contaminated by clouds and are removed. To implement this second cloud-filtering criterion, the range of cos (Z) between 0 and 1 was divided into 10 intervals of 0.1, and the visible reflectance values were binned for each cos (Z) interval. A specified fraction of these binned values with the highest reflectance was assumed to be cloudy; using a fraction prevents all the samples for a given cos (Z) range from being removed. For this study this fraction was set rather arbitrarily to 50%, which is strict but which lowers the probability of retaining cloudy samples. Figure 3 shows the reflectance values for the samples remaining at several buoys, for which the satellite-based filtering is employed, after the first filtering condition has been applied. The black dots in Figure 3 denote the samples that were filtered, and the shaded dots are those samples that were retained as the result of applying the

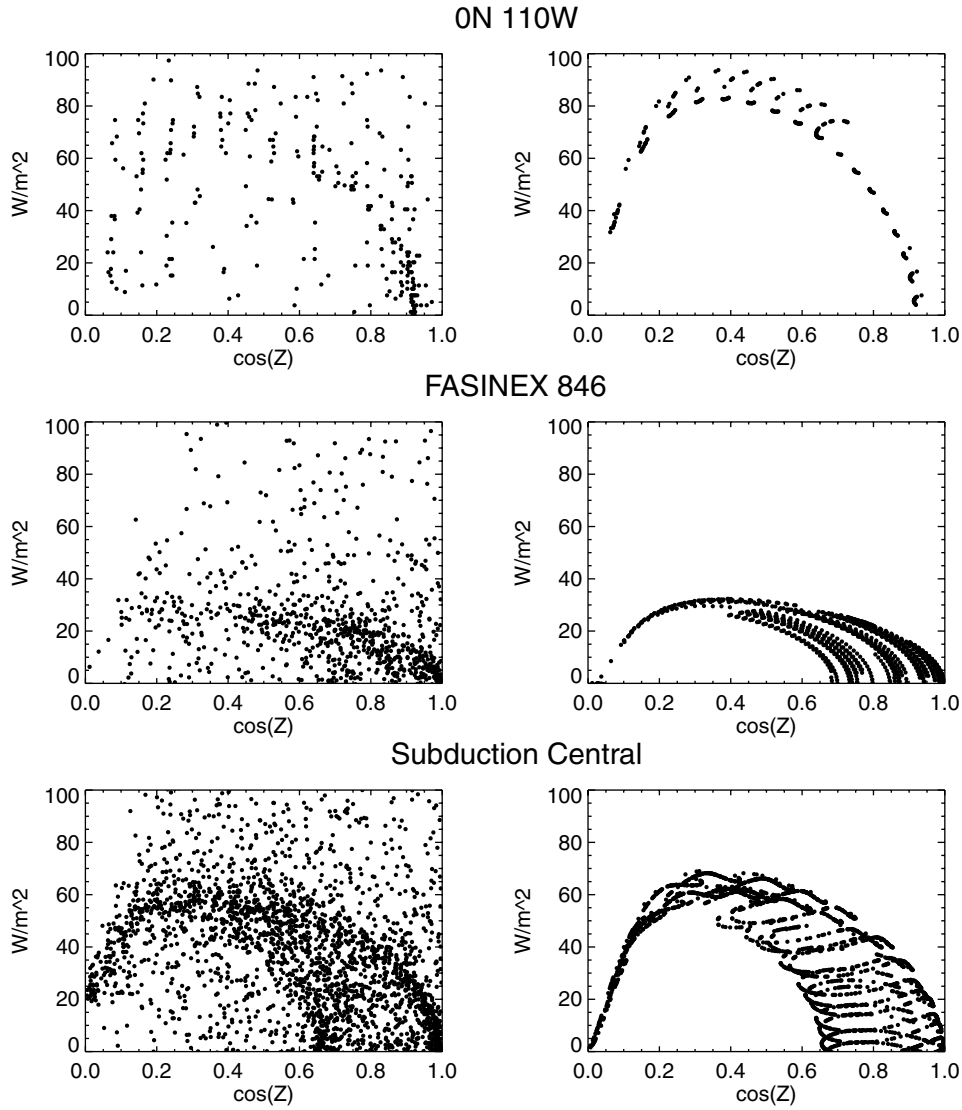

Figure 4. Observed (left) and estimated (right) changes between subsequent and previous buoy SW samples for TAO 0n110w, FASINEX 846, and central Subduction buoys plotted against the cosine of the solar zenith angle. Samples in these plots are those remaining after the cloud flag and reflectance cloud filtering steps have been performed.

second criterion. This is a more generalized version of the second criterion applied by *Waliser et al.* [1999].

[15] Figure 2c shows the remaining samples versus cos (Z) after the second criterion has been performed for the FASINEX 846 buoy. There are still a number of samples that appear to be associated with clouds, making additional filtering necessary. The third screening step provides an additional criterion that discards samples if the change in their insolation values with respect to the previous or subsequent values differs significantly from the expected change in the surface insolation over that same time interval. The reasoning is that under clear skies the observed values change rather slowly, and abrupt changes would be expected to be associated with cloudy conditions. For this criterion the expected change is found by calculating the top-of-the-atmosphere (TOA) SW radiation and then, on the basis of this value, computing an estimate of the change of surface SW radiation transmitted from the TOA. The changes in these estimated insolation values with respect to the previous and subsequent values are then computed and compared to the changes in the actual observed insolation. Values that have an unexpectedly high sample-to-sample change are discarded. The theoretical formulation for SW radiation received at the surface [e.g., *Sparrow and Cess*, 1966] can be expressed as

$$Q = Q_o \exp\left(-\tau_{o/} \cos\left(Z\right)\right), \tag{1}$$

where Q_o is the SW flux received at the TOA; τ_o is optical depth of the atmosphere; and cos (Z) is cosine of solar zenith angle. We have computed an average τ_{O} for each buoy using the observations for all samples remaining after the first and second criteria were applied (i.e., for supposedly clear-sky values):

$$\langle \tau_o \rangle = \langle \cos\left(Z\right) \ln\left(Q_o/Q\right) \rangle. \tag{2}$$

This averaged $\langle \tau_o \rangle$ was then used in (1) to calculate the expected transmitted SW, Q.

[16] The plots of the modeled surface SW changes and the buoy-observed SW changes between present and subsequent samples (7.5-, 15-, or 20-min interval depending on the buoy) for several buoys are shown in Figure 4. For the most part, the changes in

Table 1. Summary of Satellite-Based and Empirical Cloud-Filtering Criteria Applied to Buoy-Measured Shortwaves Values[a]

	Satellite-Based Filtering Results					Empirical Filtering Results		
Buoy/Experiment	All Samples Before Any Filtering	Criterion 1 ISCCP DX Cloud Flag	Criterion 2 Lower Visible Reflectance	Criterion 3 Sample-to-Sample Change	Criterion 4 Gross Error Check[b]	All Samples Before Any Filtering	After Idealized Shortwave Selection	After Gross Error Check[b]
FASINEX 845	14680	4029	1844	503	503	14680	669	669
FASINEX 846	14806	4193	1916	668	665	14806	748	747
FASINEX 847	13867	3909	1790	521	520	13867	564	563
FASINEX 848	13814	3938	1797	741	739	13814	897	896
FASINEX 849	12791	3543	1621	411		12791	1213	
MLML	8757	941	299	127	127	8757	328	320
Subduction, central	34931	13631	5940	2517	2512	34931	1452	1451
Subduction, northeast	34941	11094	4564	2092	2070	34931	1452	1451
Subduction, northwest	19948	6334	2649	1218	1214	34941	1298	1296
Subduction, southeast	29286	11299	5288	2435	2386	29286	1226	1224
Subduction southwest	24370	9504	3855	1522	1511	24370	965	958
TOGA COARE	12501	2216	1079	274	269	12501	455	447
0n110w, TAO	3112	1715	849	378	375	15351	407	407
0n140w, TAO	25298	15252	5733	2504	2493	47090	1284	1281
0n156e, TAO	14342	2642	1297	317	311	27337	297	295
0n165e, TAO	3323	369	176	45	44	19490	269	269
Arabian Sea						35721	2384	2372
PACS, north						24437	213	213
PACS, south						24824	582	582
Biowatt						26952	1217	1217

[a] Each column shows the number of samples remaining after the column's clear-sky filtering criterion is applied to the buoy data. Note that the number of initial samples for TAO buoys in the satellite-based method is less than in the empirical method because of unavailability of International Satellite Cloud Climatology Project (ISCCP) DX data after 1994.

[b] These columns show the final number of samples.

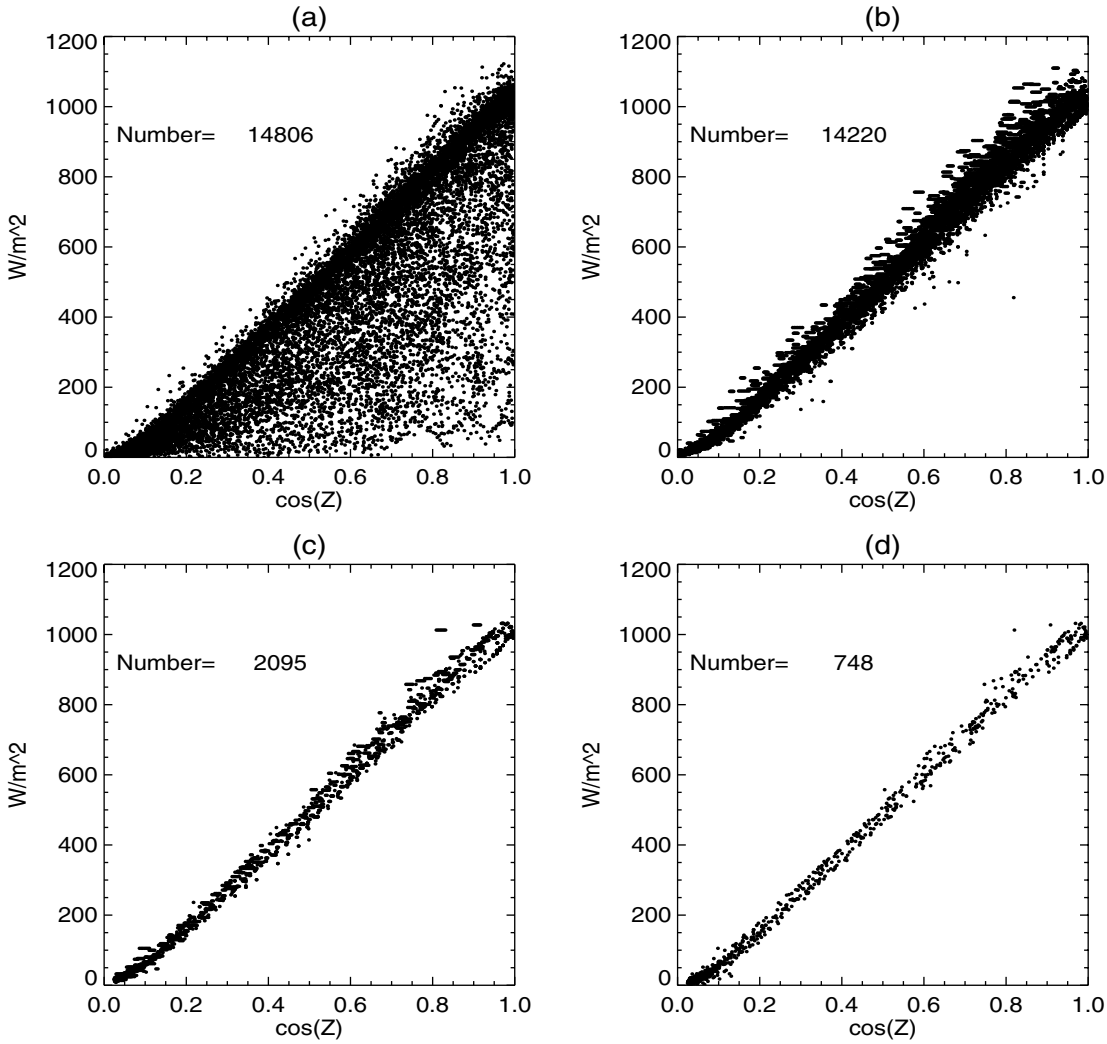

Figure 5. SW samples from the FASINEX 846 buoy plotted versus the cosine of the solar zenith angle at various stages of the empirical cloud-filtering scheme: (a) initial samples available before any filtering, (b) maximum SW of samples from 7-day intervals, (c) maximum SW of samples remaining after linear fit criterion, and (d) samples remaining after selection against the maximum SW in Figure 5c. See section 3.1.2.

calculated transmitted SW show fairly good agreement with the typical changes in observed clear-sky SW, thus allowing for the implementation of this criterion. SW samples were then discarded if the ratio of the observed change and the expected change in SW differed from 1.0 by 50% or more. Figure 2d shows the remaining samples after this criterion is performed for FASINEX 846 buoy. Overall, it is clear from Figure 2 that satellite cloud detection plays a major part in filtering the cloudy samples and that lowering the reflectance values along with sample-to-sample change criterion further refine the time series to separate out the clear-sky samples.

[17] After the three criteria have been applied, there is still evidence of a few outliers in the remaining samples that suggests some remaining cloud-contaminated values. In order to filter these out, a regression of the normalized insolation values is made versus cos (Z), and then any value that deviates from this regression by >125 W m^{-2} is also discarded. This value was chosen somewhat arbitrarily, sufficiently small to eliminate some very evident outliers and sufficiently large to retain values that have a large scatter but that still might represent clear-sky conditions. In most cases the number of samples discarded is on the order of ~10 (~1%), though the number ranges from 0 to 49. The remaining scatter in the cloud-screened fluxes at each value of cos (Z) is believed to be due to optically thin or sparsely scattered clouds that were not filtered out by the above cloud-screening procedures, due to water vapor or aerosol variations, and possibly due to the measurement error itself (e.g., errors associated with buoy tilting or with contaminants on the sensor). Table 1 shows the results of the above filtering procedures for several of the buoy locations.

3.1.2. Empirical cloud filtering. [18] The second filtering method of identifying clear-sky samples from buoy SW time series does not rely on any secondary data source and thus is more empirical in nature. First, observations from each seven consecutive days are pooled to select the maximum irradiance at each sample time during the day. This part of the procedure is similar to the approach used by *Bishop et al.* [1997]. This procedure is performed in order to construct a data set of values that most likely represent clear-sky irradiances for comparison with actual observations. These maximum irradiances, hereinafter called the "idealized values," are assigned to the middle day of each of the 7-day periods, that is, to day 4. The next 7-day period is obtained by sliding the 7-day window 1 day forward, so that each 7-day period contains 6 days from the previous 7-day period plus a new day.

[19] Figure 5a shows the initial SW samples for the FASINEX 846 buoy. Figure 5b shows the idealized values for this buoy as described above: essentially, the maximum values for every 7-day

interval. Since the 7-day periods are chosen by sliding the window by 1-day intervals, it is possible to have the same value chosen as the idealized up to 7 times. This explains the short horizontal lines in Figure 5b. The high values in Figure 5b are likely to be attributed to side-lit clouds, and the low values are likely to be associated with cloudy conditions at a particular time of the day that were persistent for an entire 7-day period. Thus additional constraints need to be applied in order to filter out these anomalous values.

[20] In the second step the idealized values from each 7-day period are checked for cloud-contaminated values. The procedure is based on the fact that SW radiation has a maximum during the day at local noon and gradually increases in the morning and decreases in the afternoon. The morning-afternoon symmetry expected from a clear-sky day can be illustrated by plotting the SW versus cos (Z) for a given day. In the case of clear-sky conditions this gives a near-linear relationship, whereas if the day were cloudy, the points would not fall on the straight line. In order to separate the clear periods from cloudy skies in the buoy data sets, one obvious approach would be to select only those days when the regression of daily SW against cosine of zenith angle has a small standard deviation, as was done by *Jing and Cess* [1998]. However, this method eliminates the whole day even if only a portion of it is cloudy. Our goal is not to identify completely clear-sky days but any clear-sky periods, even if they consist of only a few samples. Thus, in this study, a piecewise regression is applied, using just three consecutive points at each given time to determine the clear-sky status of the central point. Given the relatively high temporal resolution of sampling, we would expect any three consecutive points on a plot of cos (Z) versus SW to fall, within a very close approximation, along a line if these points represent clear-sky observations. Thus, for this filtering criterion each middle point of any three consecutive idealized values is required to lie approximately on the line drawn through the previous and subsequent points. The values are discarded if the difference between the middle point and the expected value in it is more than a defined threshold. The expected value of the middle point is calculated from the equation of a line passing through the first and the third points:

$$\mathrm{SW}_2 = \mathrm{SW}_1 + (\mathrm{SW}_3 - \mathrm{SW}_1)/(\cos(\mathrm{Z}_3) - \cos(\mathrm{Z}_1))\,(\cos(\mathrm{Z}_2) - \cos(\mathrm{Z}_1)). \quad (3)$$

Then the difference between this estimated value and the actual value in the middle point is checked against the threshold: |estimated SW - idealized SW| < threshold. Furthermore, the slope of the line for each three points is required to be positive. The threshold limit for discarding the middle of the three points is an average standard deviation of a typical clear-sky day. It is determined by analyzing the standard deviations of the SW plotted against cosine of zenith angle for several clear-sky days from FASINEX, since it has one of the most frequent samplings (7.5 min), and thus it provides the highest accuracy in estimation of the SW clear-sky daily variability. The average standard deviation about a least squares fit of the above data for a typical clear-sky day found during FASINEX data is 5 W m^{-2}, and this value is taken as the threshold for this criterion.

[21] The last step in this procedure is to use the filtered idealized values to select those observations that do not differ significantly from their corresponding clear-sky idealized values. The criterion for selection is determined by the natural variability of clear-sky SW over 3 days since this variability is imbedded in the idealized values. The reasoning for this follows from the fact that the maximum SW in each 7-day period could come from any day in this interval and still be assigned to day 4, so that the difference between the actual observation on that day and the idealized value is in part due to the expected natural variation between 2 days differing by an interval of 0–3 days. To minimize the discrepancy between the actual and idealized values and still allow for this natural difference, the threshold of the selection is set to be the average difference between the top-of-the-atmosphere SW radiation on the fourth day of each 7-day period and its first and seventh days. Figure 5d shows the filtered SW observations after the above filtering criterion has been applied for FASINEX 846. After the three criteria have been performed, there are still some outliers in the remaining samples, as was the case for the satellite-based procedure. In order to filter these out, the same gross error check applied in that screening procedure is employed here; that is, a regression of the insolation values is made versus cos (Z), and then any value that deviates from this regression by >125 W m^{-2} is discarded. However, it should be noted that examination of the data prior to applying this criterion is important for highlighting a particular type of buoy-related error, as will be shown in section 4.1.

[22] Table 1 shows the number of samples that are filtered because of this method for several buoys. The percentage of the remaining samples is ~4%. This number is similar to the outcome of the satellite-based procedure. This similarity in the overall number remaining after the two cloud-filtering schemes have been performed provides some confidence in the robustness of the two methods.

3.2. Modeled Values

[23] The modeled clear-sky flux values were computed using the single-column radiation model [*Briegleb*, 1992] from the National Center for Atmospheric Research (NCAR) Community Climate Model version 3 (CCM3) [*Kiehl et al.*, 1996]. In these calculations the solar spectrum is divided into 18 discrete spectral intervals (seven for O_3, one for visible, seven for H_2O, and three for CO_2), and the atmosphere is divided into 17 atmospheric layers ranging from 10 to 1000 mbars (the same levels used in the National Centers for Environmental Prediction (NCEP)/NCAR reanalysis [*Kalnay et al.*, 1996]). The model employs two-stream delta-Eddington approximation for evaluating the reflectivity and transmissivity for each layer in the vertical. The layers then are combined, which allows evaluation of upward and downward spectral fluxes at each interface boundary between layers. The CCM3 radiation scheme is a significant improvement from the highly parameterized methods that use bulk expressions for gaseous absorption, such as previous versions of the model: CCM0 and CCM1 [*Briegleb*, 1992]. The above features allow the CCM3 radiation code to accurately compute absorbed solar radiation in comparison to available reference calculations (line-by-line) and observations [*Briegleb*, 1992].

[24] The ancillary data sets that are necessary for model input include precipitable water, ozone profile, relative humidity in the lowest model layer, and surface pressure. Precipitable water vapor time series for all buoys, except for FASINEX and Biowatt experiments, were obtained from the Defense Meteorological Satellite Program Special Sensor Microwave Imager (SSM/I) measurements and the algorithm of *Wentz et al.* [1986]. The SSM/I orbital/swath data were composited into daily maps with 1° spatial resolution, and the water vapor time series were taken from the grid points nearest to the mooring locations. Since the SSM/I mission started only in July 1987, the precipitable water for FASINEX and Biowatt were taken from the NCAR/NCEP reanalysis. The mixing ratio in the lowest model layer is specified from the buoy observations, and the remaining water vapor is distributed upward through the model layers at the same constant mixing ratio value until no water vapor remains. The sensitivity of the calculations to this assumption is examined by *Waliser et al.* [1999], who found that it influenced the results by ~0.5% or less (~2.5 W m^{-2}). The surface pressure is taken from buoy observations where available or from NCEP/NCAR reanalysis in the case of TAO moorings. The ozone profile is taken from a 12-month, zonally averaged climatology [*Grose and Gille*, 1996]. The modeled aerosol effects are based on a sulfate aerosol, which is nearly

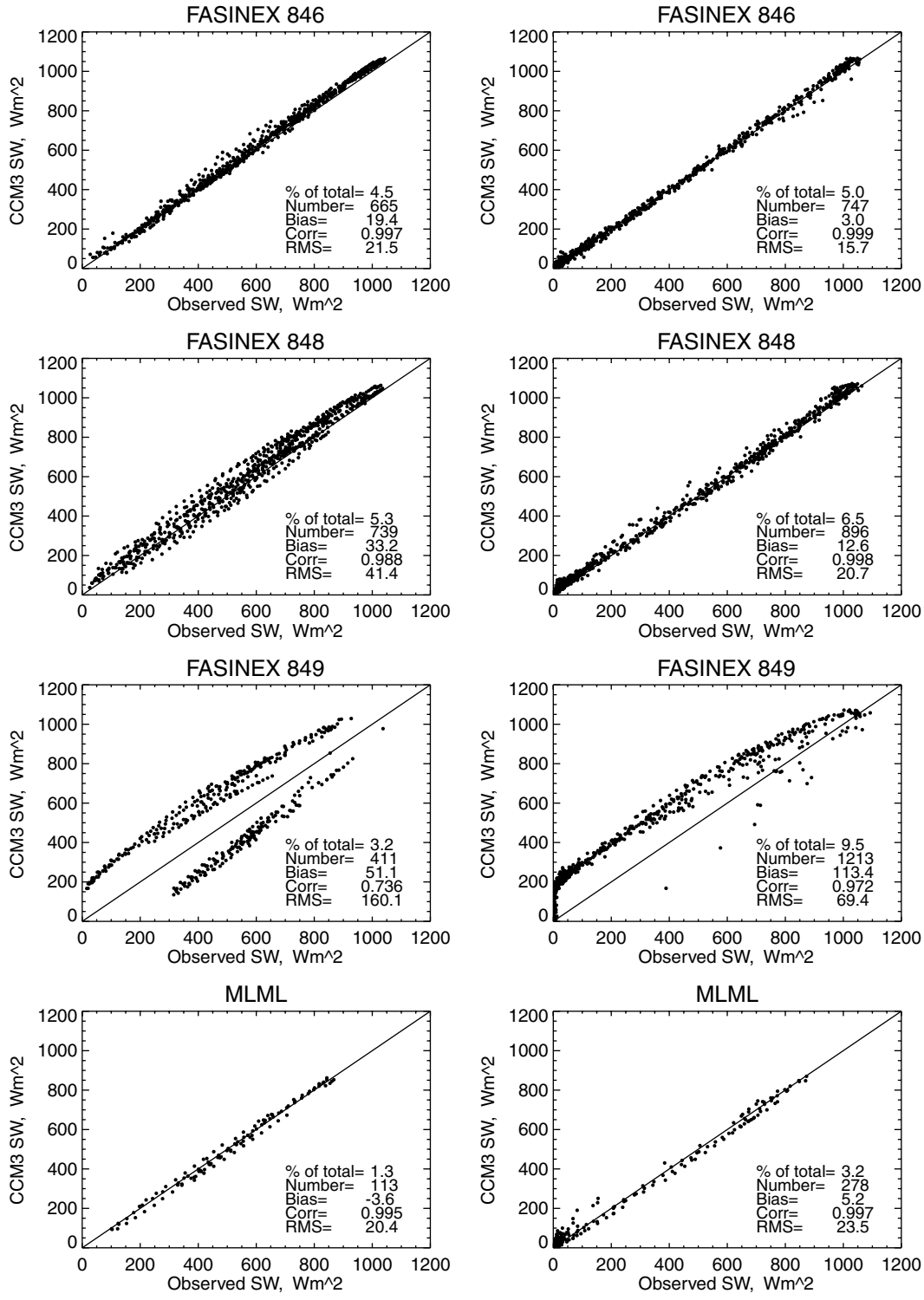

Figure 6. Model-observed SW for clear-sky samples derived from the satellite-based (left) and empirical (right) cloud-filtering methods for several buoys. Each plot contains information on (1) percentage of the total number of samples in available record; (2) number of clear-sky samples; (3) mean bias, (number of samples: CCM – Observed;); (4) correlation coefficient; and (5) RMS difference, $[(\text{CCM} - \text{Observed})^2 - \text{bias}^2]^{1/2}$. Solid lines represent perfect agreement between the two sets of values.

conservative in the visible range and modestly absorbing in the near infrared. The value of the aerosol optical thickness in the model calculations is specified to be 0.12 (a typical value for oceans [*Kiehl et al.*, 1998]). This is the only variation, not accounted for in this model, since aerosol is assumed to be a constant value. This issue is a drawback in the model calculations, and its implications will be analyzed in sections 4.2 and 4.3.

[25] The confidence in the CCM3 clear-sky calculations is supported by numerous studies in validating the radiative transfer scheme of this model to several observational data sets [e.g., *Cess et*

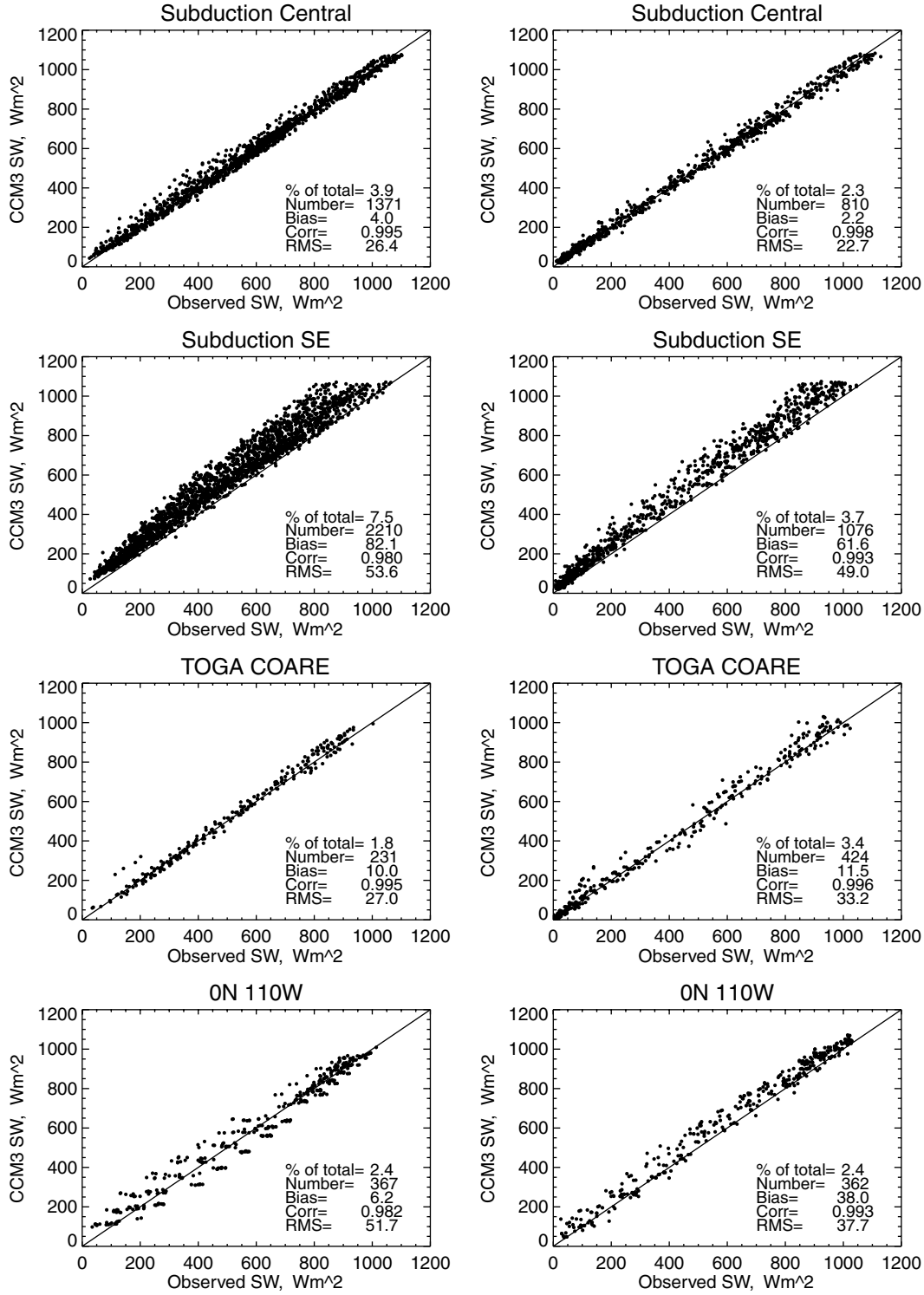

Figure 6. (continued)

al., 1996; *Zender et al.*, 1997; *Chou and Zhou*, 1997; *Jing and Cess*, 1998; *Zhang et al.*, 1998]. *Cess et al.* [1996] performed a comparison between clear-sky SW observations from Boulder Atmospheric Observatory and NCAR CCM2 (which employs the same radiation scheme as CCM3, except for the explicit treatment of aerosol). Their analysis shows the agreement between model calculations and observations to be within 0.3%. *Jing and Cess* [1998] used hourly averaged clear-sky surface insolation measurements from 24 Canadian stations and the NCAR CCM3 radiation code, and they found bias error between modeled and observed values to be ~0.8% (~3 W m^{-2}). *Zender et al.* [1997] conducted their study using data from the ARM Enhanced Shortwave Experiment (a site over Oklahoma) for September–November 1995. They found agreement between observed and modeled clear-sky data to be about the value of instrumental uncertainty, i.e., ~1%. In addition, *Chou and Zhou* [1997] employed SW data from several island stations and a buoy that were part of the TOGA COARE radiation measurement program in the western Pacific. Using the same radiation scheme as

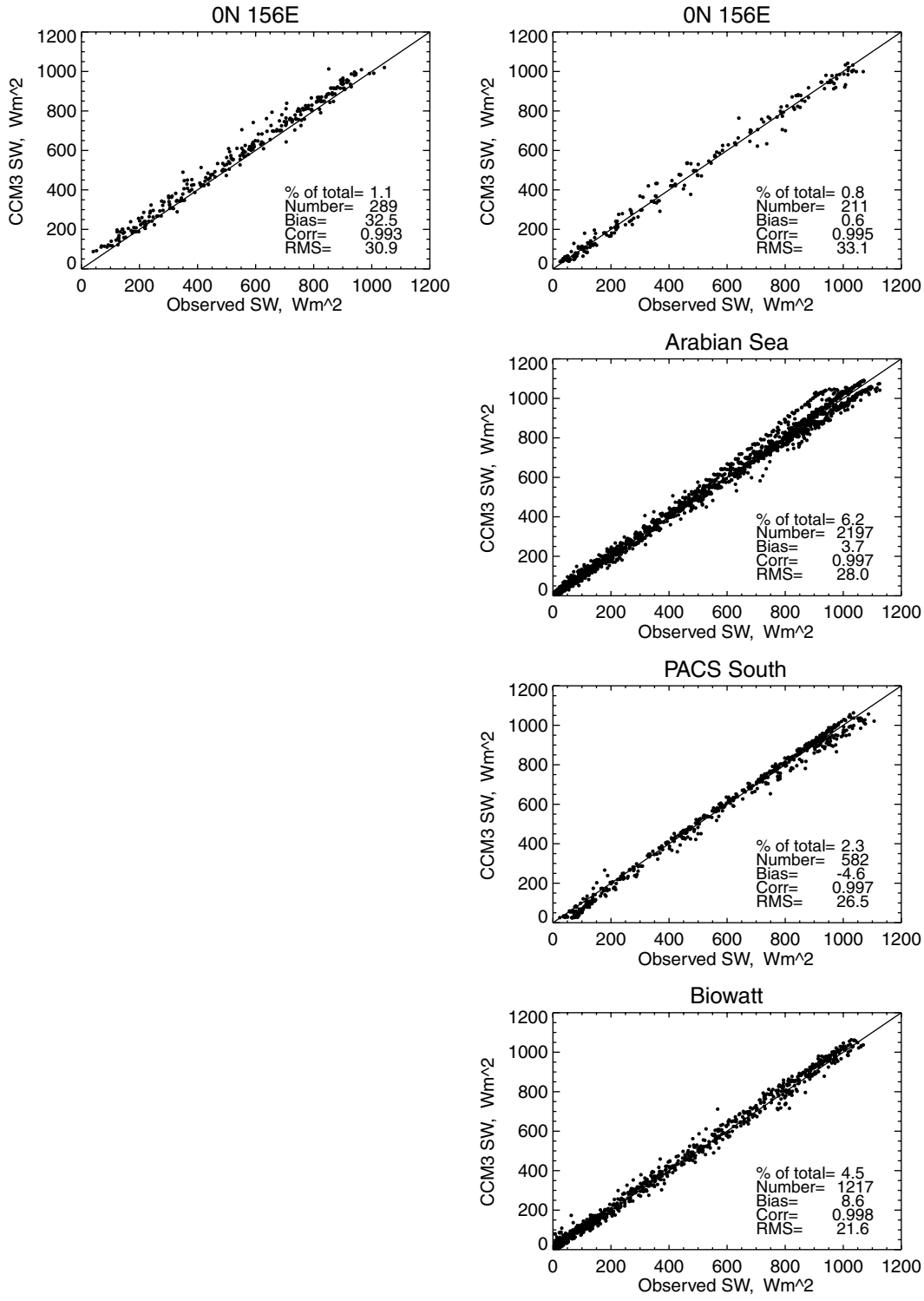

Figure 6. (continued)

in this study, they found disagreement between the clear-sky observations and modeled values to be <0.7%.

[26] Nearly all of the studies cited above employed land-based observations. The quality of the measurements taken from land-based sensors is likely to be much higher than that of measurements taken from a moving/rocking buoy in the open ocean that is likely to receive little or no maintenance during its deployment (a matter of months). In this respect, we would consider the typical agreement found in the studies mentioned above to represent an upper limit to the level of agreement we might expect from model-data comparisons using buoys. In addition, if the comparisons for a given buoy show discrepancies significantly different from this level of agreement, its data should probably be utilized with caution.

4. Modeled Versus Observed

[27] Clear-sky values were computed with the CCM3 model for the clear-sky buoy samples derived from the two different filtering

techniques. The number of clear-sky samples available for model-data comparisons from either filtering method has been reduced because of missing water vapor values and/or because of missing meteorological information (e.g., relative humidity) that is required for the model calculations [see *Medovaya*, 1999, Table 4].

[28] Figure 6 shows the agreement between the model-calculated and observed surface SW values for a number of buoys (see *Medovaya* [1999] for the rest) for clear-sky periods filtered by the satellite-based (left panels, where applicable) and empirical methods (right panels). Qualitatively, the results from both methods are similar to each other for each particular buoy. Note that the satellite-based filtering tends to eliminate the SW values at low cos (Z). This is because of the third criterion in the satellite-based procedure (i.e., sample-to-sample change), since the expected calculated change in the surface insolation is inherently different from the observed change because of high uncertainties in calculating the optical depth τ_O and parameterizing the transmitted incoming solar radiation at these angles [*Cess and Vulis*, 1989; *Cess et al.*, 1993]. The empirical method is not prone to this behavior and thus retains more low cos (Z) values. From Figure 6 the question arises of how similar are the two filtering methods and how dependent are the overall results on the filtering scheme employed. In section 4.1 the comparison of the two filtering methods is performed.

4.1. Comparison of the Filtering Methods

[29] To compare the results from the two filtering methods, Figure 7 shows bar charts that depict CCM-observed biases, root-mean-square (RMS) differences, and the numbers of samples used in CCM-observed analysis for all buoys. The buoys in Figure 7 are assembled in three groups according to the availability of satellite data. These groups are separated by solid black lines: the bottom portion contains buoys which provided the same time series for each cloud-filtering method; the middle portion includes TAO 0n110w, 0n140w, and 0n156e buoys which had truncated time series in the satellite-based filtering; the top portion shows buoys which were subject to only empirical cloud filtering because of the lack of satellite data. We can make direct comparisons of how the two methods perform by looking at the bottom portion of the charts in Figure 7 that show the buoys which were subject to both filtering methods using the same length time series. From the bias and RMS charts it can be seen that the two methods produce similar results for most of these buoys, taking into account that the bias values within the ± 10 W m^{-2} interval (dashed lines in Figure 7a) are considered to be small and insignificant since this number is of the same order as the typical calibration error of the buoy observations (see section 2 as well as *Cess et al.* [1996], *Conant et al.* [1997], *Zender et al.* [1997], and *Jing and Cess* [1998]). Similarly, RMS values below 30 W m^{-2} (dashed lines in Figure 7b) are also considered to exhibit reasonable agreement given the uncertainties associated with the cloud screening, model calculations, and buoy environment/platform (see sensitivity calculations by *Waliser et al.* [1999]).

[30] Significant differences between the two cloud-filtering methods are most evident for the FASINEX moorings: the biases and RMS differences for the results of satellite-based cloud filtering are higher than those for the results of empirical filtering. One possible reason for these differences is that the satellite-based filtering might be retaining some SW values contaminated by very thin cloud layers that were not identified by any of the filtering criteria associated with satellite cloud detection. A more peculiar problem appears in the comparisons for FASINEX 848 and 849. Figure 6 shows that these buoys exhibit similar "ellipsoidal" behavior, which suggests that daily morning observations systematically differed from afternoon observations. For the case of SW data coming from a truly clear-sky period, the satellite data (i.e., cloud flag and reflectance) would not indicate cloudy conditions, and thus these SW samples would be retained. However, the empirical method will be more likely to filter these samples out since they might not show a linear relationship with cos (Z), a requirement for clear-sky samples in the empirical procedure (i.e., second criterion). This ellipsoidal behavior suggests that there might have been a problem with the pyranometer tilt on the buoy mast. In this case we see how employing two different cloud-filtering methods can help to identify a problem as well as suggest a possible cause of the model-data discrepancies. Note that the final step of filtering cloudy samples (threshold of 125 W m^{-2} deviation from least squares fit) was not performed for the FASINEX 849 buoy to illustrate its unusual behavior.

[31] Despite the modest differences in the results of the two cloud-filtering schemes, Figure 6 and Figure 7 show that both of the methods point out suspicious observations. Among the buoys that had the same length time series subject to both filtering methods, several buoys can be identified as problematic based on their relatively high biases and high RMS differences in the results from both methods: FASINEX 849 and 848 and the southeast and southwest Subduction buoys. The nature of the problems associated with these buoys will be discussed in more detail below.

[32] Given that both schemes tend to identify the highly problematic cases, this provides us confidence in using either method alone to examine the rest of the buoys in Figure 7 (middle and top portions of the bar charts; see Figure 7 caption). In these cases, the buoys that exhibit high model-data bias and RMS values are 0n110w and 0n140w TAO buoys and north PACS. The other two TAO buoys, 0n156e and 0n165e, might seem problematic as well, but note that these buoys provide a rather small number of samples (especially 0n165e), which might result in less representative values of bias and RMS. Also, in the case of 0n156e buoy, the bias is appreciable only for the satellite-based filtering. The rest of the buoys show relatively small bias and RMS differences for both filtering methods. The buoys showing good model-data agreement are the central, northeast, and northwest Subduction, TOGA COARE, FASINEX 845, 846, and 847, Biowatt, MLML, Arabian Sea, and south PACS.

[33] Having identified a number of buoys that show poor model-data agreement, it is of interest to determine the likely sources of the model-data discrepancies. These discrepancies can be due to either the shortcomings in our analysis or the problems with the buoy measurements. In sections 4.2 and 4.3, possible reasons for discrepancies between model and data will be discussed and considered as they might apply to specific buoys, especially those buoys which have been identified in this section as possibly problematic.

4.2. Model-Data Discrepancies Associated With Analysis Method

[34] Explanations for the model-data discrepancies that could be associated with the analysis method fall into two categories: problems related to cloud-filtering schemes and to the model. Problems with the cloud-filtering scheme would result if any unfiltered clouds remained in the clear-sky data set. These unfiltered clouds would lower the average of the buoy-observed, supposedly clear-sky samples so that the model-data bias would be high and positive. However, having two very different cloud-screening techniques that conservatively screen out $\sim$95% of the observations makes it unlikely that the cloud contamination is present in both cloud-filtering methods. Thus, for the buoys with similar values of bias and RMS in the results from both filtering methods, it is unlikely that the cloud-screening method(s) are a dominant source of model-data discrepancy.

[35] The problems associated with the CCM3 model include a number of uncertainties such as unaccounted for aerosol and ozone variability and the source and specification of water vapor. The study of *Waliser et al.* [1999] presents a sensitivity

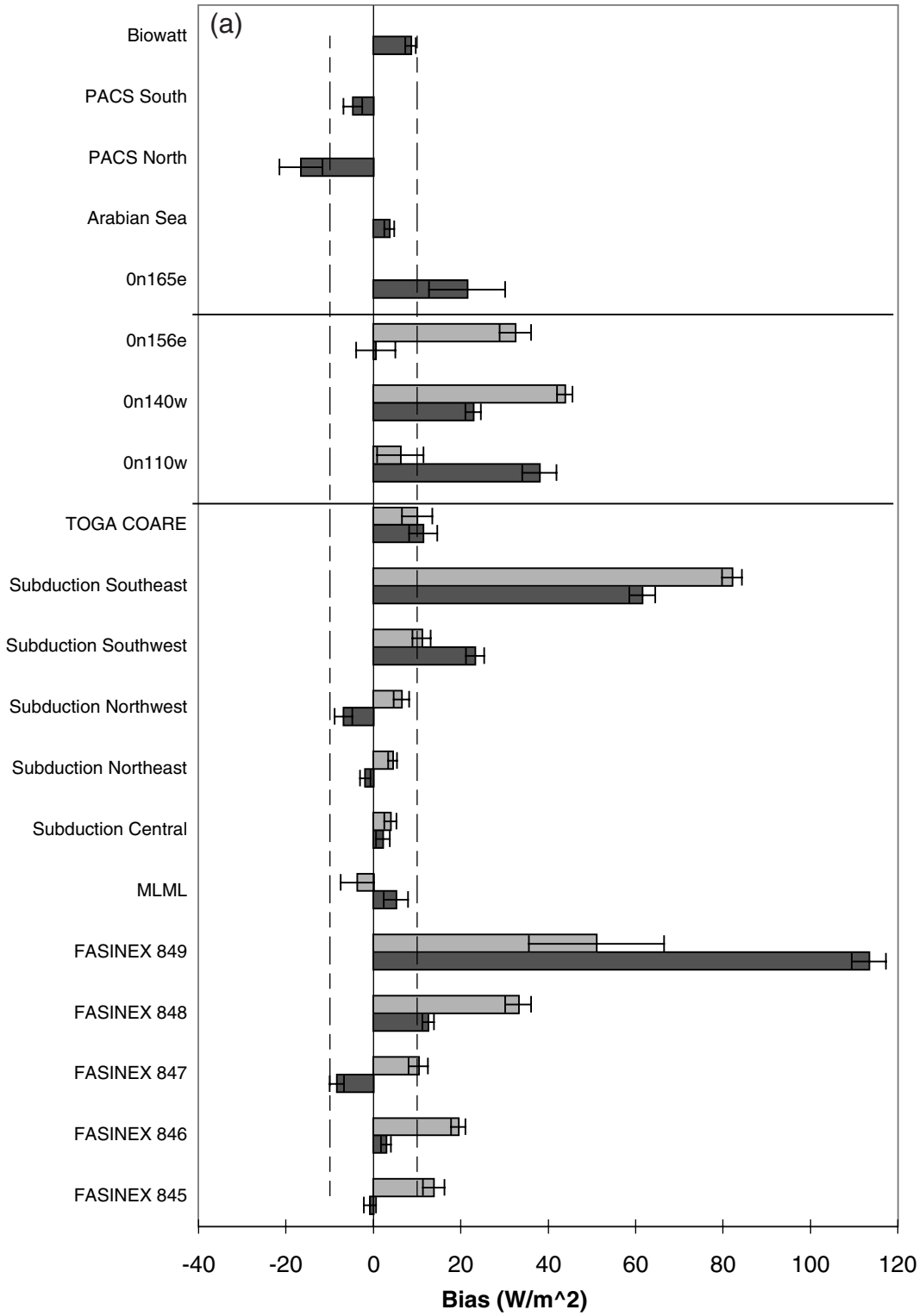

Figure 7. Summary of the model-observed clear-sky SW from the two cloud-filtering methods: (a) model-observed bias, (b) model-observed RMS difference (bias removed), and (c) number of samples used in the clear-sky model-observed comparisons. Shaded (black) bars denote the satellite (empirical) cloud-filtering scheme. Error bars are 95% confidence levels on the mean. Solid lines divide the bar chart into three categories of buoys: those that had the same length time series for both cloud-filtering methods (bottom); those that had only a limited time series for satellite-based filtering (middle); and those that did not have overlapping satellite retrievals (top). Dashed lines Figures 7a and 7b represent very rough limits for acceptable/expected model-data difference.

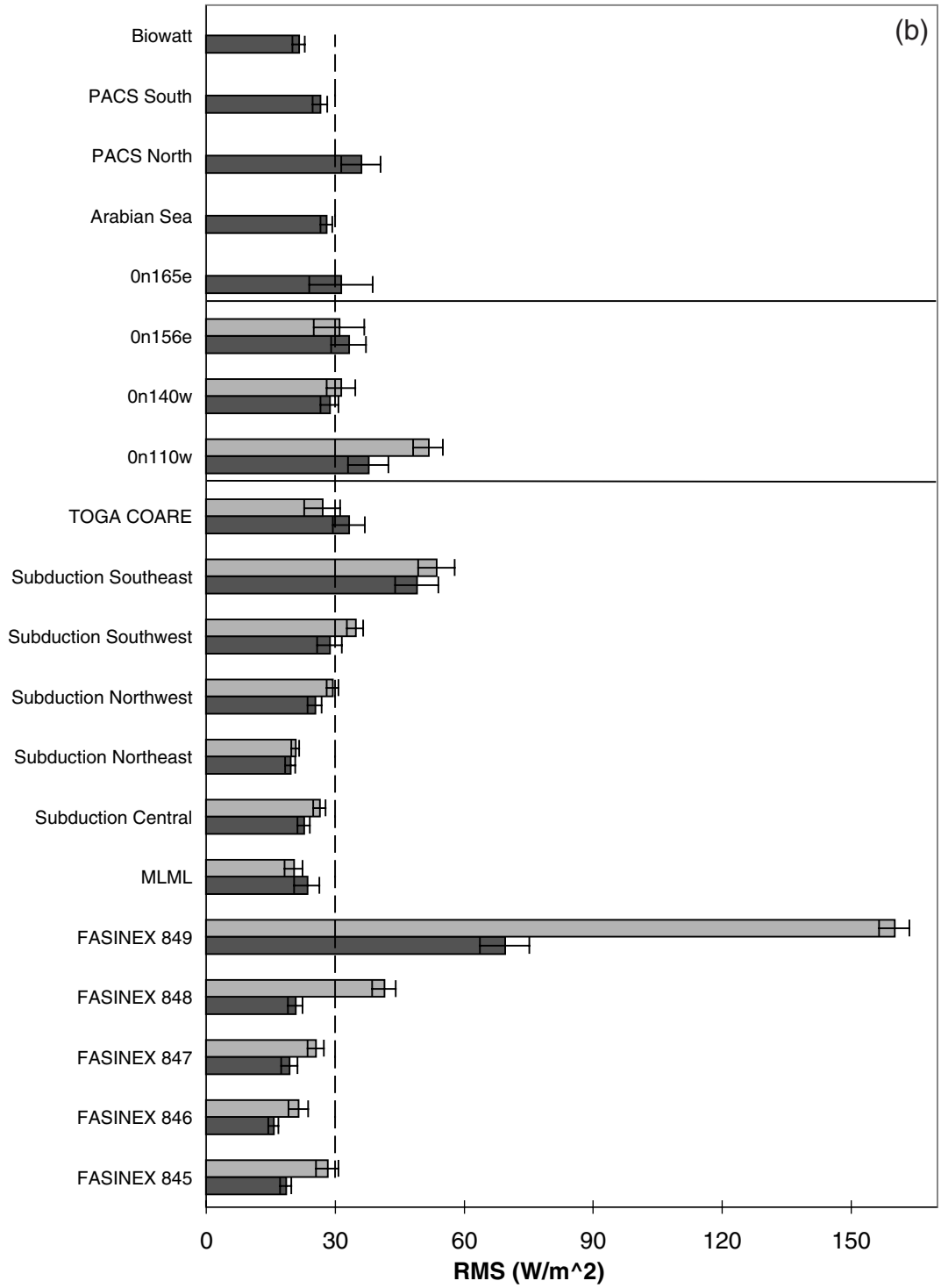

Figure 7. (continued)

analysis of the CCM3 modeled values versus Subduction Experiment data where they found that the sensitivity of the model to typical uncertainties in surface albedo (which influences the radiation reflected up from the surface and backscattered back down to the surface), column ozone, total column water vapor, and the assumed manner in which the water vapor distributed in the column result in <1% change in the level of model-data agreement. However, according to their calculations a 50% change in aerosol optical thickness, which is not that conservative given the uncertainties associated with modeling and observing aerosols, results in 1–2% change in the model-data biases, or $\sim$10 W m^{-2}.

[36] The greater dependence in the bias values for the aerosol indicates that apart from buoy-related problems it may be a dominant source for the bias and RMS differences between the observed and calculated values shown in Figure 7 for some buoys. In order to examine this possibility, daily advanced very high resolution radiometer (AVHRR) retrievals based on the algorithm of *Stowe et al.* [1997] were employed. Maps of seasonal distribution of AVHRR aerosol optical thickness, as well as discussion of

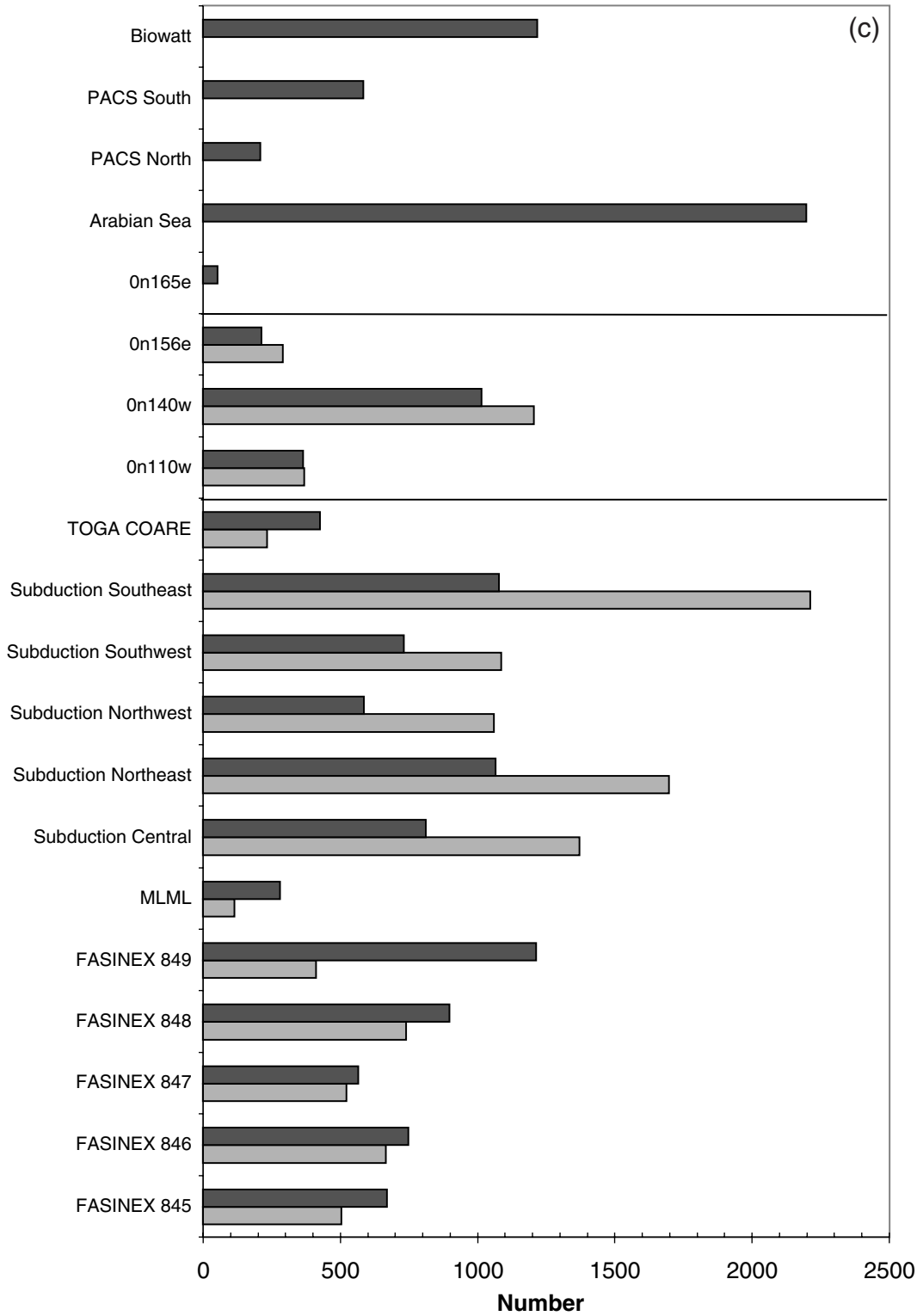

Figure 7. (continued)

their regional characteristics, can be found in the work of *Husar et al.* [1997]. In these retrievals the assumed aerosol type is best characterized as a conservatively scattering marine aerosol, which in most cases applies to the buoys discussed here. Exceptions probably include the southern Subduction buoys [cf. *Waliser et al.*, 1999], the Arabian Sea buoy, and the FASINEX buoys, all of which are probably influenced by continental aerosols. Thus, for the purposes here the AVHRR aerosol values are only serving as an indication of the actual atmospheric aerosol load.

[37] To examine the relationship between modeled-observed errors and aerosol temporal variability, time series of overlapping daily model-data bias and aerosol were analyzed. Aerosol time series colocated with each buoy were constructed from the $1° \times 1°$ grid locations nearest to each of the buoys. The available aerosol

Table 2. Correlation Coefficients Between Daily Aerosol Advanced Very High Resolution Radiometer (AVHRR) Retrievals And Daily Clear-Sky Modeled/Observed Bias Times Series[a]

	Empirical		Satellite	
Buoy	Correlation	Number	Correlation	Number
FASINEX 845	0.26	33	−0.20	12
FASINEX 846	0.16	33	0.17	13
FASINEX 847	0.28	31	0.20	13
FASINEX 848	−0.12	30	0.03	14
FASINEX 849	0.01	29	−0.18	11
MLML	0.06	21	−0.79	4
Subduction, central	(0.40)	91	(0.63)	65
Subduction, northeast	0.22	111	−0.17	61
Subduction, northwest	(0.45)	61	(0.42)	45
Subduction, southeast	0.13	93	0.12	66
Subduction, southwest	(0.29)	70	(0.71)	47
TOGA COARE	0.04	11	−0.84	6
0n110w		0		0
0n140w	(0.37)	69	(0.45)	66
0n156e	−0.38	11	0.28	14
0n165e		0	N/A	N/A
Arabian Sea		0	N/A	N/A
PACS, north	0.09	16	N/A	N/A
PACS, south	(0.40)	52	N/A	N/A
Biowatt	−0.09	57	N/A	N/A

[a] Parentheses represent statistically significant correlations at 99% level. No correlation is shown for those buoys that did not have overlapping aerosol AVHRR retrievals. N/A is assigned to those buoys that did not have overlapping International Satellite Cloud Climatology Project DX data.

retrievals have a time span of 10 years, ranging from 1986 to 1996, although 90% of the days from this period are typically missing because of AVHRR satellite sampling. The results are presented in Table 2. For several buoys in the table, 0n110w, 0n165e, and Arabian Sea buoys, there are no overlapping model-data biases and aerosol retrievals. However, it is likely that 0n110w behaves similar to 0n140w and 0n165e behaves similar to 0n156e since they are located in close proximity. The fact that a number of sites show a positive, and somewhat expected, relation between aerosol and model-data SW bias time series can help to explain a portion of the RMS differences, since large temporal variability in aerosol would result in larger values of RMS difference. Such may be the case for the two eastern Pacific TAO buoys and several of the Subduction buoys, for example. However, it seems clear that aerosol variability is unlikely to explain the very high RMS at FASINEX 849, and thus other factors must be playing a role. In addition, the fact that the expected positive relation does not exist at all sites in Table 2 does not necessarily mean that such a physical relation does not exist, it just means that the limited number of overlapping observations and uncertainties associated with the AVHRR product are not able to capture them. For example, one would anticipate such a relationship for the southeast Subduction buoy where the aerosol load is quite high and variable. However, as discussed by *Waliser et al.* [1999], the lack of a significant relationship at this site probably owes to the highly variable nature of the aerosol type over this region, which cannot be diagnosed by AVHRR alone, as well as to the deposition on the sensor itself.

[38] While temporal variability in aerosol might help explain model-data RMS differences, it would not account for variations in mean model-data bias (Figure 7a). These variations would tend to be associated with the spatial variability of the mean aerosol amount rather than with the temporal variability. To examine this question, we would need the (true) mean aerosol value for the clear-sky samples for the period of the deployment. This number is dependent on the nature of the technique used in identifying the aerosol optical depth and thus is highly uncertain. Figure 7 shows *Stowe et al.* [1997] AVHRR aerosol values versus model-data bias, both averaged over the periods of buoy deployment. Though the actual aerosol values might not be precise, as was noted above, Figure 7 points out the buoys with highly contrasting aerosol amounts and to some extent indicates a positive relation between bias and aerosol amount. This positive trend is consistent with Figure 10 of *Jing and Cess* [1998], where the authors plotted bias versus AVHRR-determined aerosol optical thickness. Both the southeast and southwest Subduction buoys lie in the region of high aerosol load, west of the Sahara desert, and each tends to have a relatively high mean bias. Thus it is likely that the model underspecifies the amount of aerosol for these sites, and their higher positive bias values would at least partly be attributed to this underspecification. Underspecification of model aerosols can play a role for the 0n110w and 0n140w TAO buoys as well because of enhanced aerosol after the 1991 Mount Pinatubo eruption. Note that normally, the tropical eastern Pacific does not have high aerosol content, and the negative bias value for the north PACS buoy is likely associated with an overspecification of aerosol. For example, their aerosol values are ~0.7, which is ~50% lower than the modeled value. On the basis of the model sensitivity calculations this would result in about a 10 W m^{-2} error, similar to what is seen here.

[39] Additional insight into the influence of aerosol on the model-data differences can be obtained by examining the time series of model-data bias in consideration with the associated changes in AVHRR aerosol amounts (not shown; see *Medovaya* [1999]). For example, consider the 0n140W TAO buoy, which shows a fairly large model-data clear-sky bias (20–40 W m^{-2}; Figure 7a). From Figure 8, there is a suggestion that its mean aerosol load might be ~50% higher than the typical oceanic (and model-specified) value. This would suggest that at least 10 W m^{-2} (25–50%) of this bias is probably the result of an underspecification of aerosol in the model at this location. A large portion of this bias comes from the period 1991 to ~1993, which coincided with the period of enhanced atmospheric aerosol due to the 1991 Mount Pinatubo eruption [*Russell et al.*, 1996]. Apart from the above sorts of anomalous variations, there is also evidence of seasonal influences of aerosol on the model-data differences. The most pronounced is seen in the evolution of the model-data clear-sky biases for the Arabian Sea buoy. During most of the year the air over this region is fairly pristine [*Husar et al.*, 1997], and the model-data bias is slightly negative. However, during the Northern Hemisphere autumn, there is a pronounced increase in both the aerosol

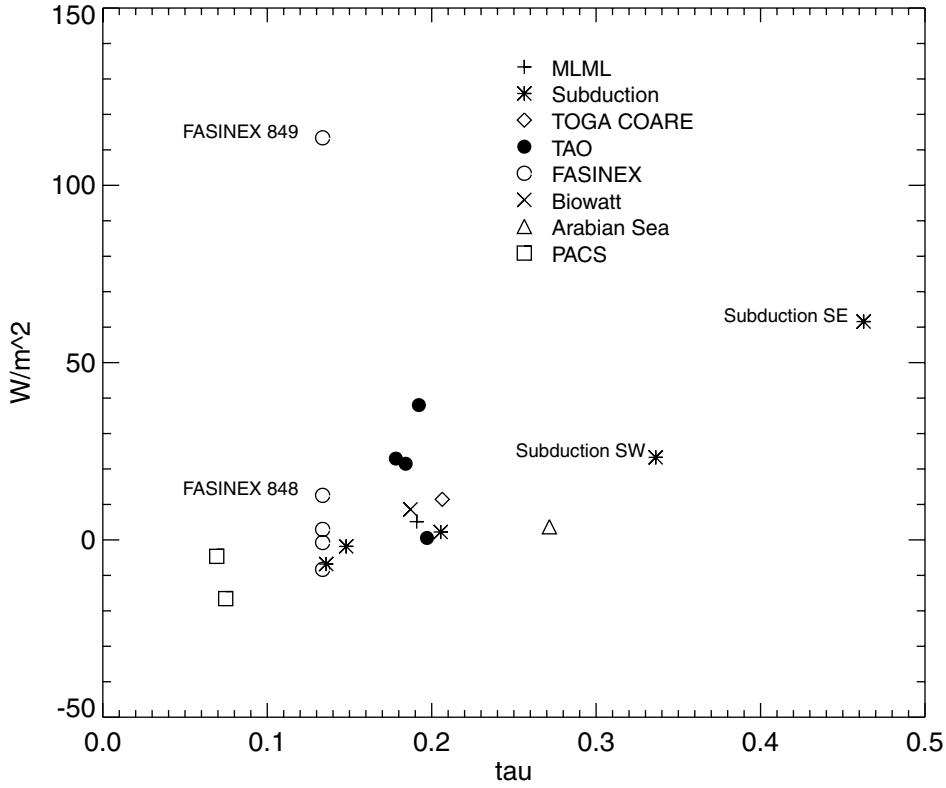

Figure 8. Mean clear-sky model minus observed clear-sky SW bias versus mean aerosol optical depth for the period of buoy record.

amount and the model-data bias. While this case demonstrates the influence of aerosols on the evolution and simulation of the SW, it appears that over the course of the deployment the model-data bias is rather small because of the cancellation between periods of low (underspecified) and high (overspecified) aerosol.

[40] On the basis of the above analysis and discussion it appears that the relatively high biases for the southeast and southwest Subduction, 0n140w, and 0n110w TAO buoys, as well as for the north PACS buoys, are due at least in part to the overspecification or underspecification of aerosol optical thickness in the model. The slightly higher RMS difference for these sites, particularly for the southwest Subduction, 0n140w, and possibly 0n110w buoys, might also be due to unaccounted temporal aerosol variability in the model. In addition, while a site like the Arabian Sea does not show a large mean model-data bias, the specification of a constant aerosol amount is influencing the seasonal evolution of the model-data discrepancy and is likely contributing to the size of its RMS difference as well [see *Medovaya*, 1999]. Given the uncertainties associated with observing and modeling aerosols, it is impossible for the above analysis to determine the absolute fraction of the discrepancy associated with aerosol. Rather, it can simply point to the likelihood of aerosols playing a significant role and thus remove an unnecessary caution with respect to a given buoy exhibiting relatively high model-data disagreement.

4.3. Model-Data Discrepancies Associated With the Buoy or Environment

[41] Sources of buoy- or environment-related errors may include (1) buoy tilt due to the winds or ocean currents; (2) SW sensor tilt due to problems associated with either buoy adjustment (tilt of the hull) or the adjustment of the sensor itself on the buoy mast; or (3) aerosol/salt buildup on the sensors. There are other possible sources of buoy-related errors, the worst one being problems with the SW sensor, but in this analysis we will limit ourselves to a qualitative consideration of only the three categories listed above.

[42] Typically, the pitching and rocking of the buoy hull is small, as the tension (typically 907.2 kg) in the mooring line where it attached to the bridle on the underside of the buoy hull provides a large righting moment. However, previous analytic [*Katsaros and De Vault*, 1986] and laboratory [*MacWhorter and Weller*, 1991] studies have shown that while time average errors (e.g., hourly or longer averages) due to buoy rocking motion tend to be small, errors due to mean tilts can be significant when tilting toward or away from the sun changes the apparent zenith angle. According to the sensitivity studies by *Waliser et al.* [1999], in the case of a mean buoy tilt of only 1° the changes to the clear-sky biases are on the order of 2–3%, or ~10–15 W m^{-2}. These results suggest that buoy tilt due to ocean current variability is likely playing a role in the RMS differences between modeled versus observed values. However, without further information on the actual buoy tilt as a function of time, it is hard to quantify this influence, although some qualitative considerations can be made in terms of the relationships between model-data discrepancies and the associated wind and currents values.

[43] In the wind analysis the bias and RMS differences for each buoy were plotted against the speed and direction of the surface wind for each clear-sky data point (see *Medovaya* [1999] for details). These scatterplots showed evidence of higher positive bias and higher RMS differences when there is a combination of persistence of the wind direction and a relatively high speed: for example, eastern TAO (trades), southwest and southeast Subduction (trade), and Arabian Sea (southwest monsoon) buoys. These results indicate that in some cases, winds might influence the quality of the SW data measured at the buoys. However, given the small surface area profile of the buoy and the large tension of the mooring line, it is expected that the wind is actually influencing the model-data discrepancies by introducing swell which would

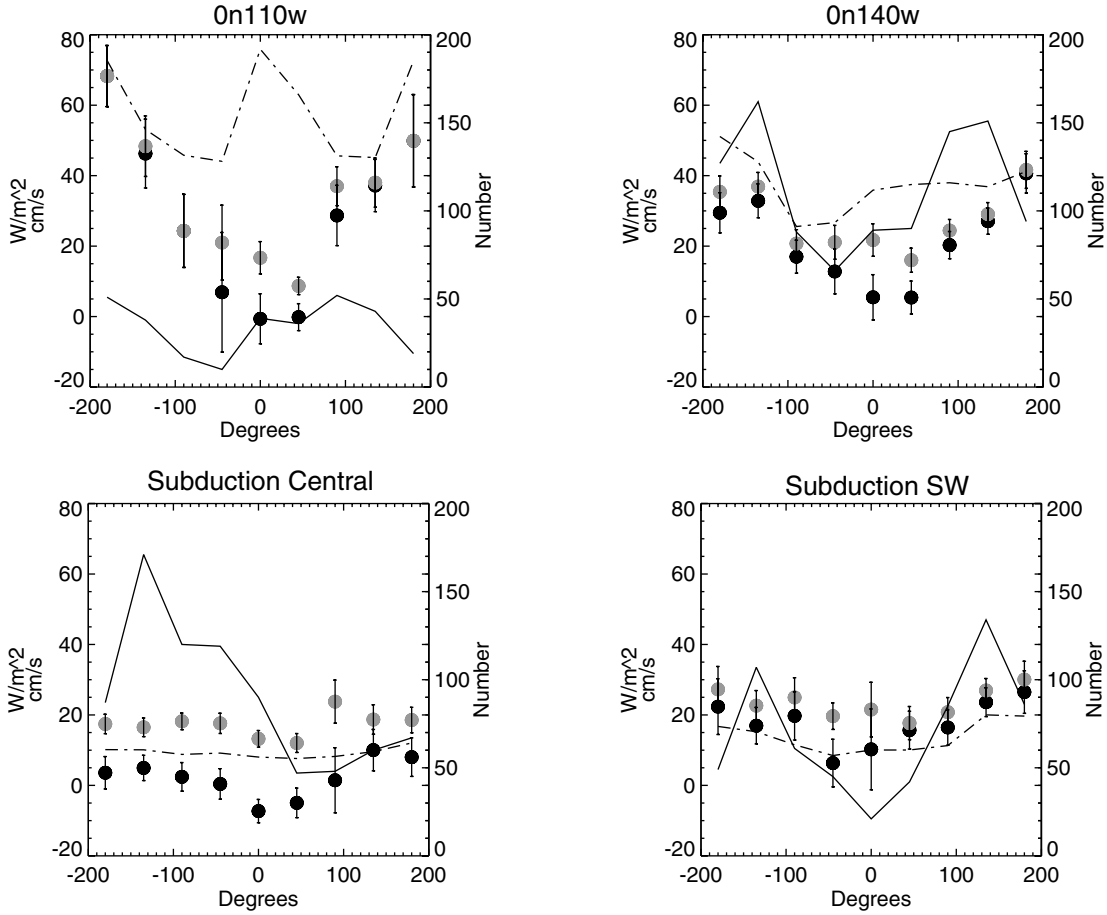

Figure 9. Clear-sky model minus data SW bias (black dots), RMS (shaded dots), and current speed (dash-dotted line) plotted against ocean current direction at 10 m for several buoys (values given on left axis). Error bars are confidence intervals at 95% level. Number of samples in each bin is denoted by the solid line (values given on right axis).

primarily affect the RMS values and/or by introducing mean currents which could lead to a mean tilt via the interaction between the current, hull, and mooring line.

[44] To examine the relation between currents and model-data bias and RMS, the bias, RMS difference, and number of samples were plotted against current direction and magnitude for the Subduction and eastern Pacific TAO buoys. Figure 9 shows a subset of the results of bias (black dots; left axis), RMS (shaded dots; left axis), speed (dash-dotted line; left axis), and number of samples (solid line; right axis) plotted against current direction (0° is eastward, 90° is northward, 180° and −180° are westward, and −90° is southward). Most evident are relatively large changes in bias (∼30–60 W m^{-2}) between eastward and westward currents for two eastern Pacific TAO buoys, with similar although weaker (∼10–15 W m^{-2}) variations for the southwest Subduction buoy as well. On the basis of these data it seems that strong and/or persistent currents might be influencing the model-data bias and RMS values, most likely through the development of a tilt to the buoy via drag on the mooring line and hull. In the case of the 0n110w TAO buoy, there is less persistence of direction than for the other buoys shown but the currents are strong (∼70 cm s^{-1}) in both the eastward and westward directions, which suggests larger drag and different tilts for these two current directions. For the 0n140w TAO buoy the bias and RMS values increase in association with westward currents, which tend to be the most frequent and have higher speeds (∼40 cm s^{-1}). A similar situation appears to occur for the southwest Subduction buoy, although the effect seems to be diminished because of the weaker current speeds (∼15 cm s^{-1}). Finally, for the more poleward central Subduction buoy, there seems to be very little impact on model-data differences from the currents; overall, this is presumably due to the weaker current speeds and associated weaker drag.

[45] It is possible that the SW sensor can be adjusted on the buoy mast with an inclination away from the vertical or that the buoy hull can be tilted because of problems not associated with wind/ocean-induced stress. This appears to be the problem with FASINEX 848 and 849. These two buoys show similar peculiar ellipsoidal behavior over the course of the diurnal cycle (Figure 6, satellite-based filtering) which seems to be an indication of large discrepancy between daily morning and afternoon observations (see section 4.1 for discussion) and possibly an indication of a tilt error. This feature is most likely attributed to a bias in the pyranometer viewing angle so that morning observations would systematically differ from the afternoon ones. Such a systematic bias would result from an east-west tilt to the sensor. This tilt could be due to the tilt of the buoy itself (probably associated with the mooring) or to an inclination of the pyranometer itself, which is installed on the buoy mast. Given that the rotation of the buoy around its own (vertical) axis would tend to be limited by the bridle attachment of the mooring and the preferred environmental current direction, it is possible that a given tilt could be maintained for lengthy periods of the deployment. In any case, the results above point to the problems with the SW observations from these buoys, particularly those in relatively clear skies.

[46] Aerosol and salt accumulation on the pyranometers can be a large source of error in the SW measured at the buoys, especially in the areas of high aerosol load and/or low rainfall amount. As was discussed in section 4.2, the two Subduction buoys with high amounts of aerosols are the southeast and southwest buoys. For these buoys the likely explanation for the high model-data bias as well as for the RMS differences is the underspecification of the (constant) aerosol optical depth in the model. On the other hand, considering the high aerosol load and low rainfall at these sites, we can suspect that the aerosol accumulation on the sensors of these buoys may also be a possible explanation [*Waliser et al.*, 1999]. Other buoys for which this might present a problem are those in the equatorial eastern Pacific Ocean, since there is a higher than average aerosol load in the Northern Hemisphere fall which happens also to be a time of low rainfall.

5. Conclusions

[47] The goal of this study was to assess the surface shortwave (SW) observations measured in situ by open-ocean buoys in a manner that would allow an independent check of the data throughout the deployment periods, as opposed to the typical calibration analysis performed before and after buoy deployments. The analysis was based on the comparison of buoy-measured SW against radiative transfer model calculations, provided in this study by the single-column radiation code from the NCAR Community Climate Model, version 3 [*Kiehl et al.*, 1996]. The purpose of this comparison is to use the model calculations as a uniform benchmark to identify the discrepancies between the model-derived and the buoy-measured SW. Only clear-sky values were employed, since the model's clear-sky radiation has been found to be a robust calculation (e.g., land-based studies by *Cess et al.* [1996], *Zender et al.* [1997], *Chou and Zhou* [1997], and *Jing and Cess* [1998]). Sensitivity studies from previous investigations show that the only significant source of uncertainty in the model clear-sky SW calculations, when used in this fashion, is unaccounted for aerosol variability (spatial, temporal, and type), since the model is typically employed using a fixed aerosol optical depth typical of oceanic conditions. Thus, for buoys located in typical aerosol conditions the model calculations are reliable in representing the clear-sky SW radiation, and any discrepancies between modeled and observed values would be more readily attributed to errors associated with the buoy sampling.

[48] The buoy data employed for this study come from several experimental and operational deployments conducted by Woods Hole Oceanographic Institution (WHOI) and Pacific Marine Environmental Lab (PMEL). Two different cloud-filtering procedures were developed to isolate the clear-sky SW values. For each clear-sky observed SW sample, modeled values were calculated, and comparisons between the modeled and observed values were then carried out using primarily mean bias and RMS difference measures. The results from these comparisons were used to distinguish buoys which appeared to have reliably measured the surface SW from those that may have been subject to difficulties associated with their environment or deployment (e.g., sensor tilt, aerosol build up, or buoy tilt/rocking).

[49] Attempts were first made to attribute any model-data discrepancies to unaccounted aerosol variability, since it is the only significant shortcoming associated with the model calculations as employed in this context. For several buoys, high positive bias ($\sim$20 W m^{-2} or higher) or large RMS ($\sim$30 W m^{-2} or higher) were associated with relatively high aerosol value or temporal aerosol variability, and for those the cause of the model-data discrepancies is presumed to be unaccounted for aerosol variability (amount, type, etc.) in the model calculations (e.g., southwest and southeast Subduction and TAO 110°W and 140°W buoys). However, given the uncertainties associated with both observing aerosols (types, sizes, and amount) and modeling their radiative interaction, it is presently not possible to quantify the amount of discrepancy actually associated with the aerosols, although it is safe to say that the model-data differences and uncertainties introduced by aerosols are of the same order of magnitude. It is also important to note that in some cases the aerosol problem even extends to the likelihood of significant buildup on the sensor itself (e.g., southeast Subduction buoy [*Waliser et al.*, 1999]). This, of course, would not be considered a problem with the analysis but rather with the difficult nature of the observing environment.

[50] Apart from the considerations of the model/analysis shortcomings the approach discussed above leads to the identification of a number of buoys that do not appear to have any obvious or significant problems related to their SW observations. These are the central, northeast, and northwest Subduction, MLML, Arabian Sea, TOGA COARE, TAO 0n156e, PACS, Biowatt, and FASINEX 845, 846, and 847 buoys. From the buoys analyzed, this leaves three of the TAO buoys, the southwest and southeast Subduction buoys, and the FASINEX 848 and 849 buoys. One of the TAO buoys, 0n165e, did not provide enough clear-sky samples to make very conclusive statements about the character of the model-data discrepancies. For the two eastern Pacific TAO buoys, 0n140w and 0n110w, and the southwest and southeast Subduction buoys the results are a bit mixed. There is reason to believe that part of the model-data discrepancies associated with these buoys might be explained by the aerosol treatment in the model calculations. However, analyses of the bias and RMS differences versus near-surface currents indicate that some of the disagreement may be associated with the interactions between the platform and the environment (e.g., currents). Such a result is not completely unexpected, as idealized calculations show that even a 1° tilt can induce an error of 2–3% ($\sim$10–15 W m^{-2}) in measurements of clear-sky surface SW [e.g., *Katsaros and De Vault*, 1986; *MacWhorter and Weller*, 1991; *Waliser et al.*, 1999]. However, the impact of the currents on buoy SW observations via hull tilt have never been quantified or substantiated in actual field observations. Results from this study indicate that the impact might possibly produce mean bias errors as large as 20 W m^{-2} or more. However, it is important to emphasize that this sort of error is largely confined to clear skies, since clouds make the radiation field more diffuse and thus significantly reduce the impact of a mean tilt.

[51] The most problematic buoys identified by the analysis are FASINEX 848 and 849. These two buoys indicate errors associated with the buoy data that are most likely due to tilting of the buoy or the pyranometer itself, apart from any interaction with currents or other environmental feature (e.g., winds). Although most of the buoys analyzed by the above methods were not found to have any significant shortcomings, the level of model-data agreement is less than the level found for similar studies using land-based observations. For example, the typical size of the bias found in the present study is $\sim$10 W m^{-2} (absolute values of model-data bias averaged over all buoys and two cloud-filtering methods, but not including FASINEX 848 and 849 and southeast Subduction buoys) and $\sim$3 W m^{-2} in land-based studies [i.e., *Cess et al.*, 1996; *Chou and Zhou*, 1997; *Jing and Cess*, 1998]. This difference is somewhat expected considering the harsh environment of the buoys' locations and lack of frequent maintenance. However, it is comforting to see that the level of disagreement is not drastically different and that significant progress has been made in measuring SW over the open ocean.

[52] Overall, this study offers two contributions. The first is the finding that when the bulk of the buoy SW data are subjected to the sort of independent test developed in this study, the majority of the deployments appear to have obtained sound data, whose uncertainties do not seem altogether different from that obtained from land-based sensors. There are two aspects to this statement that are worth highlighting. First, the test applied in this study has been made possible because of the radiation community's success at modeling clear-sky radiation and, to some extent, because of the

availability of high-resolution satellite data for cloud filtering. Second, the results imply that as long as the needed accuracy is not less than a few percent, data obtained from these platforms appear generally reliable. These statements are important and very welcome news. Considered in conjunction with the level of agreement found for the few cases where satellite-derived and buoy-observed SW values have been compared [e.g., *Bishop et al.*, 1997; *Waliser et al.*, 1999], this finding implies that the three building blocks of future global flux observing schemes, the in situ time series, satellite retrievals, and GCMs, are converging, at least in certain instances.

[53] The second contribution of this study is the development of an additional method to qualitatively assess the reliability of buoy-observed SW time series, one that focuses on the in situ performance as opposed to the more conventional predeployment and postdeployment calibration tests. As the environmental conditions of the buoy are stressful and nearly impossible to recreate in a laboratory, having such an alternative method is highly useful. For example, postdeployment calibration checks would not be able to highlight problems related to sensor tilt such as that which was indicated for FASINEX 848 and 849. Moreover, they would not be able to give any indication of the types of biases that may be induced by the local current variability and its interaction with the hull. While the analysis method was developed here to perform diagnostic evaluation on archived data sets, it is also well suited for providing a real-time monitoring capability of the SW data quality. For example, if such a scheme were in place, it might be able to indicate fouling conditions or calibration drift of the sensor, as well as the developments of a tilt to the buoy/sensor that might be brought about by damage to the mooring assembly or to the buoy itself via extreme weather conditions or vandalism. One shortcoming of the method is the lack of high-quality aerosol data over the oceans that are needed for input into the radiative transfer model. Once such data become available, the method can be used with greater confidence.

[54] While the overall assessment of the buoy observations is positive, the fact that there were a number of uncertainties remaining for some buoys that cannot be well quantified implies that further research and development is needed in the area of moored observations of SW radiation. Uncertainties related to currents, wind, or some sort of mooring/sensor mount damage would be best dealt with by having information on buoy tilt. Uncertainties related to aerosol/salt buildup on the sensor would be best reduced by the presence of some sort of in situ cleansing system. Another alternative for the latter would be to have some sort of onboard internal target with a known signal, although the difficulties of developing such a mechanism seem at least as if not more formidable than implementing a cleansing system. In any case, as rain provides a natural remedy to this problem in many instances, the development of a tilt "sensor" is deemed the highest priority for reducing the remaining overall uncertainties associated with buoy-observed values of surface SW.

[55] **Acknowledgments.** Support for this study was provided by the Radiation Science Program of the National Aeronautics and Space Administration under grant NAG-1-2065 (D. W.), the Marine Meteorology Program of the Office of Naval Research under grants N00014-97-10527 (D. W.) and N00014-90- J1490 (R. W.), and NOAA's Office of Oceanic and Atmospheric Research (M. J. M.). We would like to thank Bruce Wielicki (NASA/Langley) for helping to establish this study and for providing us with a number of useful technical comments and suggestions. This study's analysis greatly benefited from the use of the TeraScan software analysis system, a product of SeaSpace Corporation, San Diego, California. We would like to thank Paul Freitag (NOAA Pacific Marine Environmental Laboratory) and Peter Furey (Woods Hole Oceanographic Institution) for helping with the buoy data and Pete Peterson (University of California, Santa Barbara) for providing the time series of SSM/I precipitable water. We would also like to thank S. Josey and an anonymous reviewer for their comments and suggestions regarding the manuscript and its presentation. The origin of this study stems from the first author's Master's thesis at the State University of New York, Stony Brook. In this regard, the first two authors would like to thank Robert Cess and Robert Wilson for their comments and suggestions regarding this work.

References

Anderson, S. P., K. Huang, N. J. Brink, M. F. Baumgartner, and R. A. Weller, Pan American Climate Study (PACS) Data Report, *Tech. Rep. WHOI-2000-03*, 145 pp., Woods Hole Oceanogr. Inst., Woods Hole, Mass., 2000.

Arking, A., The radiative effects of clouds and their impact on climate, *Bull. Am. Meteorol. Soc.*, *72*, 795–813, 1991.

Arking, A., Absorption of solar energy in the atmosphere: Discrepancy between model and observations, *Science*, *273*, 779–782, 1996.

Bishop, J. K. B., W. B. Rossow, and E. G. Dutton, Surface solar irradiance from the International Satellite Cloud Climatology Project 1983-1991, *J. Geophys. Res.*, *102*(D6), 6883–6910, 1997.

Briegleb, B. P., Delta-Eddington approximation for solar radiation in the NCAR Community Climate Model, *J. Geophys. Res.*, *97*(D7), 7603–7612, 1992.

Brink, N. J., K. A. Moyer, R. P. Trask, and R. A. Weller, The subduction experiment: Mooring field program and data summary, *Rep. 95-08*, 113 pp., Woods Hole Oceanogr. Inst., Woods Hole, Mass., 1995.

Cess, R. D., and I. L. Vulis, Intercomparison and interpretation of satellite-derived directional albedos over deserts, *J. Clim.*, *2*, 393–407, 1989.

Cess, R. D., et al., Interpretation of cloud-climate feedback as produced by 14 atmospheric general circulation models, *Science*, *245*, 513–516, 1989.

Cess, R. D., S. Nemesure, E. G. Dutton, J. J. DeLuisi, G. L. Potter, and J.-J. Morcrette, The impact of clouds on the shortwave radiation budget of the surface-atmosphere system: Interfacing measurements and models, *J. Clim.*, *6*, 308–316, 1993.

Cess, R. D., et al., Absorption of solar radiation by clouds: Observations versus models, *Science*, *267*, 496–499, 1995.

Cess, R. D., M. H. Zhang, Y. Zhou, X. Jing, and V. Dvortsov, Absorption of solar radiation by clouds: Interpretation of satellite, surface, and aircraft measurements, *J. Geophys. Res.*, *101*(D18), 23,299–23,309, 1996.

Chou, M. D., and W. Zhou, Estimation and model validation of the surface solar radiation and cloud radiative forcing using TOGA COARE measurements, *J. Clim.*, *10*, 610–620, 1997.

Clough, S. A., and P. D. Brown, Radiative transfer for clear and cloudy atmospheres: Spectral modeling and validation, paper presented at 5th ARM Science Team Meeting, U. S. Dep. of Energy, Washington, D. C., 1995.

Conant, W. C., V. Ramanathan, F. P. J. Valero, and J. Meywerk, An examination of the clear-sky solar absorption over the central equatorial Pacific: Observations versus models, *J. Clim.*, *10*, 1874–1884, 1997.

Dickey, T., et al., Seasonal variability of biooptical properties in the Sargasso Sea, *J. Geophys. Res.*, *98*(C1), 865–898, 1993.

Esbensen, S. K., and Y. Kushnir, The heat budget of the global ocean: An atlas based on estimates from surface marine observations, *Rep.29*, Clim. Res. Inst., Oreg. State Univ., Corvallis, 1981.

Freitag, H. P., Y. Feng, L. J. Mangum, M. J. McPhaden, J. Neander, and L. D. Stratton, Calibration procedures and instrumental accuracy estimates of TAO temperature, relative humidity and radiation measurements, *NOAA TM ERL PMEL-104*, 32 pp., Natl. Oceanic and Atmos. Admin., Silver Spring, Md., 1994.

Fung, K. K., and V. Ramaswamy, On shortwave radiation absorption in overcast atmospheres, *J. Geophys. Res.*, *104*(D18), 22,233–22,241, 1999.

Grose, W., and J. Gille, Upper Atmospheric Research Satellite Validation Workshop III report: Temperature and constituents validation, *NASA Conf. Publ. CP-331*, NASA, Greenbelt, Md., 1996.

Harrison, F. E., P. Minnis, B. R. Barkstrom, V. Ramanathan, R. D. Cess, and G. G. Gibson, Seasonal variation of cloud radiative forcing derived from the Earth Radiation Budget Experiment, *J. Geophys. Res.*, *95*(D11), 18,687–18,703, 1990.

Husar, R. B., J. M. Prospero, and L. L. Stowe, Characterization of tropospheric aerosols over the oceans with the NOAA advanced very high resolution radiometer optical thickness operational product, *J. Geophys. Res.*, *102*(D14), 16,889–16,909, 1997.

Jing, X., and R. D. Cess, Comparison of atmospheric clear-sky shortwave radiation models to collocated satellite and surface measurements in Canada, *J. Geophys. Res.*, *103*(D22), 28,817–28,824, 1998.

Kalnay, E., et al., NCEP/NCAR 40-year reanalysis project, *Bull. Am. Meteorol. Soc.*, *77*, 437–471, 1996.

Katsaros, K. B., and J. E. De Vault, On irradiance measurement errors at sea due to tilt of pyranometers, *J. Atmos. Oceanic Technol.*, *3*, 740–745, 1986.

Kiehl, J. T., and B. P. Briegleb, The relative roles of sulfate aerosols and greenhouse gases in climate forcing, *Science*, *260*, 311–314, 1993.

Kiehl, J. T., J. J. Hack, M. H. Zhang, and R. D. Cess, Sensitivity of a GCM climate to enhanced shortwave cloud absorption, *J. Clim.*, *8*, 2200–2212, 1995.

Kiehl, J. T., J. J. Hack, G. B. Bonan, B. A. Boville, B. P. Briegleb, D. L. Williamson, and P. J. Rasch, Description of the NCAR Community Climate Model (CCM3), *NCAR Tech. Note NCAR/TN-420*, Natl. Cent. for Atmos. Res., Boulder, Colo., 1996.

Kiehl, J. T., J. J. Hack, and J. W. Hurrel, The energy budget of the NCAR Community Climate Model: CCM3, *J. Clim.*, *11*, 1151–1178, 1998.

MacWhorter, M. A., and R. A. Weller, Error in measurements of incoming shortwave radiation made from ships and buoys, *J. Atmos. Oceanic Technol.*, *8*, 108–117, 1991.

Mangum, L. J., H. P. Freitag, and M. J. McPhaden, TOGA-TAO array sampling schemes and sensor evaluations, paper presented at Oceans '94 Ocean Space Advanced Technologies European Show, Institut Francais de Recherche pour l'Exploitation de la Mer, Brest, France, September 13–16 1994.

McPhaden, M. J., et al, The Tropical Ocean-Global Atmosphere (TOGA) observing system: A decade of progress, *J. Geophys. Res.*, *103*(C7), 14,169–14,240, 1998.

Medovaya, M., A method for assessing the integrity of ocean buoy observations under operating conditions, Master's thesis, State Univ. of N.Y. at Stony Brook, Stony Brook, 1999.

Moyer, K. A., and R. A. Weller, Observations of surface forcing from the subduction experiment: A comparison with global model products and climatological datasets, *J. Clim.*, *10*, 2725–2742, 1997.

Oberhuber, J. M., An atlas based on the COADS data set, *Rep. 15*, Max Planck Inst. fur Meteorol., Hamburg, Germany, 1988.

Ohmura, A., and H. Gilgen, Global Energy Balance Archive (GEBA): The GEBA database, interactive applications, retrieving data, *World Clim. Program Water Proj. A7 Rep. 2*, 60 pp., Verlag der Fachvereine, Zurich, 1991.

Ohmura, A., et al., Baseline Surface Radiation Network (BSRN/WCRP): New precision radiometry for climate research, *Bull. Am. Meteorol. Soc.*, *79*, 2115–2136, 1998.

Plueddemann, A. J., R. A. Weller, M. Stramska, and T. D. Dickey, Vertical structure of the upper ocean during the Marine Light-Mixed Layers experiment, *J. Geophys. Res.*, *100*(C4), 6605–6619, 1995.

Ramaswamy, V., and S. M. Freidenreich, A study of broadband parameterizations of the solar radiative interactions with water vapor and water drops, *J. Geophys. Res.*, *97*(D11), 11,487–11,512, 1992.

Rossow, W. B., and R. A. Schiffer, ISCCP cloud data products, *Bull. Am. Meteorol. Soc.*, *72*, 2–20, 1991.

Russell, P. B., et al., Global to microscale evolution of the Pinatubo volcanic aerosol derived from diverse measurements and analyses, *J. Geophys. Res.*, *101*(D13), 18,745–18,763, 1996.

Slingo, A., and J. M. Slingo, Response of the National Center for Atmospheric Research Community Climate Model to improvements in the representation of clouds, *J. Geophys. Res.*, *96*(D8), 15,341–15,357, 1991.

Sparrow, E. M., and R. D. Cess, *Radiation Heat Transfer*, 322 pp., Wadsworth, Belmont, Calif., 1966.

Spencer, R. W., Global oceanic precipitation from the MSU during 1979–91 and comparisons to other climatologies, *J. Clim*, *6*, 1301–1326, 1993.

Stowe, L. L., A. M. Ignatov, and R. R. Singh, Development, validation, and potential enhancements to the second generation operational aerosol product at the National Environmental Satellite Data and Information Service of the National Oceanographic and Atmospheric Administration, *J. Geophys. Res.*, *102*(D14), 16,923–16,934, 1997.

Waliser, D. E., W. D. Collins, and S. P. Anderson, An estimate of the surface shortwave cloud forcing over the western Pacific during TOGA COARE, *Geophys. Res. Lett.*, *23*, 519–522, 1996.

Waliser, D. E., R. A. Weller, and R. D. Cess, Comparisons between buoy-observed, satellite-derived, and modeled surface shortwave flux over the subtropical North Atlantic during the Subduction Experiment, *J. Geophys. Res.*, *104*(D24), 31,301–31,320, 1999.

Weare, B. C., P. T. Strub, and M. D. Samuel, Marine climate atlas of the tropical Pacific Ocean, *Contrib. 20*, 147 pp., Univ. of Calif., Davis, 1980.

Weller, R. A., Overview of the Frontal Air-Sea Interaction Experiment (FASINEX): A study of air-sea interaction in a region of strong oceanic gradients, *J. Geophys. Res.*, *96*(C5), 8501–8516, 1991.

Weller, R. A., and S. P. Anderson, Surface meteorology and air-sea fluxes in the western equatorial Pacific warm pool during the TOGA Coupled Ocean-Atmosphere Response Experiment, *J. Clim.*, *9*, 1959–1990, 1996.

Weller, R. A., M. F. Baumgartner, S. A. Josey, A. S. Fischer, and J. C. Kindle, Atmospheric forcing in the Arabian Sea during 1994–1995: Observations and comparisons with climatology and models, *Deep Sea Res., Part II*, *45*, 1961–1999, 1998.

Wentz, F. J., L. A. Mattox, and S. Peteherych, New algorithms for microwave measurements of ocean winds: Applications to SEASAT and the Special Sensor Microwave Imager, *J. Geophys. Res.*, *91*(C2), 2289–2307, 1986.

Zender, C. S., S. Pope, B. Bush, A. Bucholtz, W. D. Collins, J. T. Kiehl, F. P. J. Valero, and J. Vitko, Atmospheric absorption during the Atmospheric Radiation Measurement (ARM) Enhanced Shortwave Experiment (ARESE), *J. Geophys. Res.*, *102*(D25), 29,901–29,915, 1997.

Zhang, M. H., W. Y. Lin, and J. T. Kiehl, Bias of atmospheric shortwave absorption in the NCAR Community Climate Models 2 and 3: Comparison with monthly ERBE/GEBA measurements, *J. Geophys. Res.*, *103*(D8), 8919–8925, 1998.

M. J. McPhaden, Pacific Marine Environmental Laboratory, 7600 Sand Point Way NE, Building 3, Seattle, Washington 98115, USA. (mcphaden@pmel.noaa.gov)

M. Medovaya and D. E. Waliser, Marine Sciences Research Center, State University of New York, Endeavour Hall 205, Stony Brook, NY 11794-5000, USA. (medomasha@yahoo.com; duane.waliser@sunysb.edu)

R. A. Weller, Woods Hole Oceanographic Institution, Clark 204A, MS 29, Woods Hole, Massachusetts 02543, USA. (rweller@whoi.edu)